overall configuration at the Mn(1) center is also remarkable. Both the amide bonds are on one side of the manganese (cis) with an angle of 127.1 (3)° between them. This unusual coordination is, in some respects, reminiscent of the coordination seen in the metal borylamides $M(NArBMes_2)_2$ (M = Cr-Ni; Ar = Ph or Mes).[11,13,12][7] The metal coordination in these molecules is also 2-fold, but secondary interactions are observed between the metal and an ipso carbon of a boron-mesityl group so that cis structures very similar to that seen in **7** are observed. This is especially true for the Cr and Mn complexes. Another interesting feature of this structure is that if the weak coordination to N(2) is taken into account, the resulting four-coordinate structure is closer to planar coordination than it is to tetrahedral coordination. This is because the angle between the Mn(1)N(1)N(2) and Mn(1)N(1a)N(2a) planes is only 35.4°. This observation is difficult to explain since the structure is quite crowded. This crowding is evident in the bending of the aromatic rings away from each other. For example, there is an angle of 8.2° between the N(1)-C(3) bond and the plane of the C(3) phenyl ring, and an angle of 5.5° is observed between the N(2)-C(15) bond and the C(15) ring plane. This congestion might have been relieved by the adoption of a trans geometry at Mn(1) or by dispensing with the coordination of one or both of the N(2) atoms. The structure of **7** is apparently a comprise between these competing factors. Experiments on these and related ligands and their transition-metal complexes is continuing.

Acknowledgment. We thank the donors of the Petroleum Research Fund, administered by the American Chemical Society, for support of this work.

Supplementary Material Available: Tables giving full details of X-ray data collection and refinement and complete atom coordinates, bond distances and angles, hydrogen coordinates, and anisotropic thermal parameters and a drawing of the second molecule of **3** in the asymmetric unit (34 pages). Ordering information is given on any current masthead page.

(27) Bartlett, R. A.; Chen, H.; Power, P. P. *Angew. Chem., Int. Ed. Engl.* **1989**, *28*, 316.

Contribution from the Department of Chemistry, Baker Laboratory, Cornell University, Ithaca, New York 14853

Pyridine and Related Adducts, $(silox)_3ML$ (M = Sc, Ti, V, Ta): η^1-Pyridine-*N* vs η^2-Pyridine-*N*,*C* Ligation

Katharine J. Covert, David R. Neithamer, Marjanne C. Zonnevylle, Robert E. LaPointe, Christopher P. Schaller, and Peter T. Wolczanski*,†

Received October 29, 1990

Adducts of $(silox)_3M$ (M = Ta (**1**), Ti (**2**), Sc (**3**), V (**4**)) have been prepared in order to assess the various electronic factors responsible for η^1-pyridine-*N* vs. η^2-pyridine-*N*,*C* ligation. Treatment of $ScCl_3(THF)_3$ or VCl_3 with 3 equiv of Na(silox) in THF yielded $(silox)_3M(THF)$ (M = Sc (**3**-THF), V (**4**-THF)), and exposure of $[(Me_3Si)_2N]_3Sc$ to 5 equiv of (silox)H provided $(silox)_3ScNH_3$ (**3**-NH_3), but the bases could not be removed. Addition of C_2H_4, C_2H_3Me, 1-butene, and *cis*-2-butene to **1** afforded $(silox)_3Ta$(olefin) (olefin = C_2H_4 (**5a**), C_2H_3Me (**5b**), C_2H_3Et (**5c**), *cis*-MeHC=CHMe (**5d**)), although cyclometalation to give $(silox)_2HTaOSi^tBu_2CMe_2CH_2$ (**6**) competed with the latter two. In concentrated benzene solution (~0.10 M), **1** trapped C_6H_6 to yield $[(silox)_3Ta]_2(\mu\text{-}\eta^2(1,2):\eta^2(4,5)\text{-}C_6H_6]$ (**7**; ~7%) along with **6**. Acetylene, 2-butyne, and $F_3CC{\equiv}CCF_3$ reacted with **1** to give $(silox)_3Ta$(alkyne) (alkyne = C_2H_2 (**8a**), C_2Me_2 (**8b**), $C_2(CF_3)_2$ (**8c**)). Ethylene did not displace the THF and NH_3 from **3**-THF, **3**-NH_3, and **4**-THF, but reacted with **2** to provide $[(silox)_3Ti]_2(\mu\text{-}C_2H_4)$ (**9**). Treatment of **1** with pyridine, 2-picoline, 2,6-lutidine, pyridazine ($1,2\text{-}N_2C_4H_4$) and pyrimidine ($1,3\text{-}N_2C_4H_4$) provided $(silox)_3Ta(\eta^2\text{-}NC_5H_5\text{-}N,C)$ (**10a**), $(silox)_3Ta(\eta^2\text{-}6\text{-}NC_5H_4Me\text{-}N,C)$ (**10b**), $(silox)_3Ta(\eta^2\text{-}2,6\text{-}NC_5H_3Me_2\text{-}N,C)$ (**11b**), $(silox)_3Ta(\eta^2\text{-}N_2C_4H_4\text{-}N,N')$ (**12**), and $(silox)_3Ta(\eta^2\text{-}1,3\text{-}N_2C_4H_4\text{-}N^1,C^6)$ (**13**), respectively. Formation of these η^2-heterocyclic adducts is proposed to occur via nucleophilic attack by **1** at the LUMO (predominantly C=N π^*) of the substrate, a process consistent with the generation of the pyridyl hydride $(silox)_3Ta(H)(C_5H_2Me_2N)$ (**11a**) from 2,6-lutidine prior to equilibration with **11b**. Similar treatments of **2** yielded $(silox)_3Ti(\eta^1\text{-py})$ (**2**-py) and related η^1-py derivatives of 3,5-lutidine (**2**-3,5-$NC_5H_3Me_2$), 4-picoline (**2**-4-NC_5H_4Me), and 4-$NC_5H_4{}^tBu$ (**2**-4-$NC_5H_4{}^tBu$). Upon application of the McConnell equation to a_H values obtained from the ^1H contact shifts of **2**-py, the following spin density probabilities were obtained: $\rho^2(2,6) = 0.13\%$; $\rho^2(3,5) = 0.01\%$; $\rho^2(4) = 0.16\%$. η^1-Pyridine adducts $(silox)_3M(py)$ (M = Sc (**3**-py), V (**4**-py)) were produced upon exposure of $(silox)_3M(THF)$ to py. Interpretation of the UV-vis spectrum of **1** and EHMO calculations of η^1 and η^2 forms of $(silox)_3Ta(py)$ provide a rationale for the variation in pyridine ligation. Of critical importance are the four-electron repulsion between the filled d_{z^2} orbital of **1** and the py N-donor orbital and the capability of pyridine to function as a good π-acceptor in the η^2-mode.

Introduction

σ-Interactions dominate the bonding in organotransition-metal complexes, but π-effects are significant, especially in complexes containing carbon-based ligands that possess a degree of unsaturation.[1] Through the use of molecular orbital theory,[2] π-interactions in organometallic complexes can be rationalized, and the bonding of complicated ligand systems can be cogently analyzed and understood. While theory has provided a basis for examining π-effects, disclosures of unusual bonding modes still provide the field of organometallics with some of its most interesting chemistry. Recently, investigations of η^2-arene complexes[3-13] have played an important role in determining the mechanisms of arene C-H bond activations.[8,9,14,15] In addition, structural and molecular orbital studies of tantalum arene complexes revealed that even the hapticity of hexasubstituted benzenes is moot;[16-18] consequently, 7-metallanorbornadienes have been proposed as intermediates in the cyclotrimerization of alkynes.[16] These and

† Alfred P. Sloan Foundation Fellow, 1987-1989.

(1) (a) Collman, J. P.; Hegedus, L. S.; Norton, J. R.; Finke, R. G. Principles *and Applications of Organotransition Metal Chemistry*; University Science Books: Mill Valley, CA, 1987. (b) Yamamoto, A. *Organotransition Metal Chemistry*; Wiley Interscience: New York, 1986. (c) Crabtree, R. *The Organometallic Chemistry of the Transition Metals*; Wiley Interscience: New York, 1988. (d) Elschenbroich, Ch.; Salzer, A. *Organometallics*; VCH Publishers: New York, 1989.
(2) For examples, see: (a) Hoffmann, R. *Angew. Chem., Int. Ed. Engl.* **1982**, *21*, 711-724. (b) Albright, T. A. *Tetrahedron* **1982**, *38*, 1339-1388 and references therein.
(3) Muetterties, E. L.; Bleeke, J. R.; Wucherer, E. J.; Albright, T. A. *Chem. Rev.* **1982**, *82*, 499-525.
(4) Jonas, K. *Angew. Chem., Int. Ed. Engl.* **1985**, *24*, 295-311.
(5) Jonas, K.; Wiskamp, V.; Tsay, Y.-H.; Krüger, C. *J. Am. Chem. Soc.* **1983**, *105*, 5480-5481.
(6) (a) Gomez-Sal, M. P.; Johnson, B. F. G.; Lewis, J.; Raithby, P. R.; Wright, A. H. *J. Chem. Soc., Chem. Commun.* **1985**, 1682-1684. (b) Deeming, A. J. *Adv. Organomet. Chem.* **1986**, *26*, 1-83.

0020-1669/91/1330-2494$02.50/0 © 1991 American Chemical Society

other compounds in which the maximum hapticity of the organic moiety is not fully utilized are of particular interest, because the binding of the transition metal perturbs the aromaticity of the hydrocarbon.

Heterocycles have also displayed unusual bonding modes as exemplified by the η^6-binding of pyridine derivatives,[19] ligands usually considered common σ-N donors.[20,21] In these laboratories, the reactivity of (silox)$_3$Ta(**1**; silox = ^{t}Bu$_3$SiO$^-$),[22] an atypical low-valent, low-coordinate early-transition-metal complex, has undergone intense scrutiny. It is a potent reductant that can cleave carbon monoxide under mild conditions (<1 atm, ~5 °C), yet does not bind common σ-donors such as phosphines or ethers.[23] In an earlier communication, **1** was reported to bind pyridine in an unusual η^2-N,C mode, producing (silox)$_3$Ta(η^2-NC$_5$H$_5$-*N,C*), and to encapsulate benzene in generating [(silox)$_3$Ta]$_2$[μ-η^2-(1,2):η^2(4,5)-C$_6$H$_6$], a species that manifests a rare μ-η^2-(1,2):η^2(4,5)-arene coordination.[24] More recently, another η^2-N,C-bound pyridine compound, (DIPP)$_2$ClTa(η^2-2,4,6-NC$_5$H$_2$^{t}Bu$_3$-*N,C*) (DIPP = 2,6-OC$_6$H$_3$^{i}Pr$_2$), has been prepared via nitrile insertion into a tantallacyclopentadiene.[25] Transients with related η^2-pyridine-*N,C* ligands may be critical to C$_\alpha$ activations,[26,27] and those with η^2-pyridine-*C,C'* ligands, to N-donor rearrangements and the formation of pyridyl complexes.[28] In order to discern the factors responsible for the unusual binding of a pyridine moiety by (silox)$_3$Ta (**1**), several related π-complexes[22] and pyridine adducts of Sc, Ti, and V have been prepared and examined. An extended Hückel molecular orbital (EHMO) analysis of the pyridine π-bonding is also presented, and a similar analysis of **1** provides a rationale for the behavior of this molecule toward σ-donors and ligands with the capability to function as π-acids.[23]

Figure 1. Probable ground-state conformations for 1-alkene (I) and *cis*-(II) and *trans*-olefin (III) complexes.

Results

(silox)$_3$M Complexes. Preparations of three-coordinate, d^2 (silox)$_3$Ta (**1**)[23] and d^1 (silox)$_3$Ti (**2**) have been previously described.[29,30] The light-blue tantalum complex (**1**) is diamagnetic, with a ^{1}A$_1$′ ground state in accord with a (a$_1$′)^2 electron configuration ((d$_{z^2}$)^2) in D_{3h} symmetry, while the orange titanium derivative (**2**) possesses a ^{2}A$_1$′ ground state attributed to population of the d$_{z^2}$ orbital. Adducts of d^0 (silox)$_3$Sc were synthesized in reasonable yield, but the removal of the donor ligands proved difficult to accomplish. Treatment of ScCl$_3$(THF)$_3$ with 3 equiv of Na(silox) in THF produced (silox)$_3$Sc(THF) (**3**-THF) in 72% yield upon crystallization from hexane (eq 1). Exposure of

$$\mathrm{ScCl_3(THF)_3} + 3\mathrm{Na(silox)} \xrightarrow[-3\mathrm{NaCl}]{\text{THF, 25 °C, 10 h}} \underset{\textbf{3-THF}}{\mathrm{(silox)_3Sc(THF)}} \quad (1)$$

$$[(\mathrm{Me_3Si})_2\mathrm{N}]_3\mathrm{Sc} + 5\mathrm{H(silox)} \xrightarrow[25\ °\mathrm{C},\ 10\ \mathrm{h}]{\text{hexane}} \underset{\textbf{3-NH}_3}{\mathrm{(silox)_3ScNH_3}} + 2(\mathrm{Me_3Si})_2\mathrm{NH} + 2\mathrm{Me_3SiOSi}^t\mathrm{Bu_3} \quad (2)$$

(7) Belt, S. T.; Duckett, S. B.; Helliwell, M.; Perutz, R. N. *J. Chem. Soc., Chem. Commun.* **1989**, 928–930.
(8) (a) Sweet, J. R.; Graham, W. A. G. *J. Am. Chem. Soc.* **1983**, *105*, 305–306. (b) Sweet, J. R.; Graham, W. A. G. *Organometallics* **1983**, *2*, 135–140.
(9) Jones, W. D.; Feher, F. J. *J. Am. Chem. Soc.* **1986**, *108*, 4814–4818.
(10) (a) Harman, W. D.; Taube, H. *J. Am. Chem. Soc.* **1987**, *109*, 1883–1885. (b) Harman, W. D.; Taube, H. *Ibid.* **1988**, *110*, 7555–7557.
(11) For substituent effects on arene binding, see: Harman, W. D.; Sekine, M.; Taube, H. *J. Am. Chem. Soc.* **1988**, *110*, 5725–5731.
(12) For related η^2-arene intermediates, see: (a) Harman, W. D.; Taube, H. *J. Am. Chem. Soc.* **1988**, *110*, 5403–5407. (b) Harman, W. D.; Sekine, M.; Taube, H. *Ibid.* **1988**, *110*, 2439–2445. (c) Harman, W. D.; Taube, H. *Ibid.* **1988**, *110*, 7906–7907.
(13) van der Heijden, H.; Orpen, A. G.; Pasman, P. *J. Chem. Soc., Chem. Commun.* **1985**, 1576–1578.
(14) (a) Crabtree, R. H. *Chem. Rev.* **1985**, *85*, 245–269. (b) Shilov, A. E. *Activation of Saturated Hydrocarbons by Transition Metal Complexes*; D. Riedel Publishing Co: Dordrecht, The Netherlands, 1984. (c) Bergman, R. G. *Science (Washington, D.C.)* **1984**, *223*, 902–908. (d) Halpern, J. In *Fundamental Research in Homogeneous Catalysis*; Shilov, A. E., Ed.; Gordon and Breach: New York, 1986; Vol. 1, p 393. (e) For a theoretical discussion see: Saillard, J.-Y.; Hoffmann, R. *J. Am. Chem. Soc.* **1984**, *106*, 2006–2026.
(15) (a) Jones, W. D.; Feher, F. J. *J. Am. Chem. Soc.* **1984**, *106*, 1650–1663. (b) Jones, W. D.; Feher, F. J. *Ibid.* **1985**, *107*, 620–631 and references therein.
(16) (a) Bruck, M. A.; Copenhaver, A. S.; Wigley, D. E. *J. Am. Chem. Soc.* **1987**, *109*, 6525–6527. (b) Strickler, J. R.; Wexler, P. A.; Wigley, D. E. *Organometallics* **1988**, *7*, 2067–2069.
(17) Arney, D. J.; Wexler, P. A.; Wigley, D. E. *Organometallics* **1990**, *9*, 1282–1289.
(18) (a) Wexler, P. A.; Wigley, D. E. *J. Chem. Soc., Chem. Commun.* **1989**, 665–665. (b) Ballard, K. R.; Gardiner, I. M.; Wigley, D. E. *J. Am. Chem. Soc.* **1989**, *111*, 2159–2162.
(19) For examples of η^6-bound pyridines, see: (a) Fish, R. H.; Kim, H.-S.; Fong, R. H. *Organometallics* **1989**, *8*, 1375–1377. (b) Davies, S. G.; Shipton, M. R. *J. Chem. Soc., Chem. Commun.* **1989**, 995–996. (c) Chaudret, B.; Jalon, F. A. *Ibid.* **1988**, 711–713. (d) Wucherer, E. J.; Muetterties, E. L. *Organometallics* **1987**, *6*, 1691–1695. (e) Dimroth, K.; Thamm, R.; Kaletsch, H. *Z. Naturforsch., B: Anorg. Chem., Org. Chem.* **1984**, *39B*, 207–212. (f) Schmidt, R. E.; Massa, W. *Ibid.* **1984**, *39B*, 212–216. (g) Morris, R. H.; Ressner, J. M. *J. Chem. Soc., Chem. Commun.* **1983**, 909–910. (h) Choi, H. W.; Sollberger, M. S. *J. Organomet. Chem.* **1983**, *243*, C39–C41. (i) Pannell, K. H.; Kalsotra, B. L.; Parkanyi, C. *J. Heterocycl. Chem.* **1978**, *15*, 1057–1081. (j) Hemberger, P. H.; Dunbar, R. C. *Inorg. Chem.* **1977**, *16*, 1246–1247. (k) Simons, L. H.; Riley, P. E.; Davis, R. E.; Logowski, J. J. *J. Am. Chem. Soc.* **1976**, *98*, 1044–1045. (l) Biedermann, H.-G.; Ofele, K.; Tajtelbaum, J. *Z. Naturforsch., B: Anorg. Chem., Org. Chem.* **1976**, *31B*, 321–323. (m) Biedermann, H.-G.; Ofele, K.; Schuhbauer, N.; Tajtelbaum, J. *Angew. Chem., Int. Ed. Engl.* **1975**, *14*, 639–640. (n) Timms, P. L. *Ibid.* **1975**, *14*, 273–277 and references therein.
(20) Tomasik, P.; Ratajewicz, Z. Pyridine Metal Complexes. In *Heterocyclic Compounds*; Newkome, G. R., Strekowski, L., Eds.; Wiley Interscience: New York, 1985; Vol. 14.
(21) (a) Reedijk, J. Heterocyclic Nitrogen Donors. In *Comprehensive Coordination Chemistry*; Pergamon Press: New York, 1987; Vol. 2. (b) For an unusual μ-η^1-py, see: Drew, M. G. B.; Mitchell, P. C. H.; Read, A. R. *J. Chem. Soc., Chem. Commun.* **1982**, 238–239.
(22) LaPointe, R. E.; Wolczanski, P. T.; Mitchell, J. F. *J. Am. Chem. Soc.* **1986**, *108*, 6382–6384.
(23) Neithamer, D. R.; LaPointe, R. E.; Wheeler, R. A.; Richeson, D. S.; Van Duyne, G. D.; Wolczanski, P. T. *J. Am. Chem. Soc.* **1989**, *111*, 9056–9072.
(24) Neithamer, D. R.; Párkiányi, L.; Mitchell, J. F.; Wolczanski, P. T. *J. Am. Chem. Soc.* **1988**, *110*, 4421–4423. Details regarding the X-ray crystal structures of (silox)$_3$Ta(η^2-NC$_5$H$_5$-*N,C*) (**10a**) and [(silox)$_3$Ta]$_2$[μ-η^2(1,2):η^2(4,5)-C$_6$H$_6$] (**7**) have been previously documented in this communication and accompanying supplemental material.
(25) Strickler, J. R.; Bruck, M. A.; Wigley, D. E. *J. Am. Chem. Soc.* **1990**, *112*, 2814–2816.
(26) (a) Klei, E.; Teuben, J. H. *J. Organomet. Chem.* **1981**, *214*, 53–58. (b) Watson, P. L. *J. Chem. Soc., Chem. Commun.* **1983**, 276–277. (c) Thompson, M. E.; Baxter, S. M.; Bulls, A. R.; Burger, B. J.; Nolan, M. C.; Santarsiero, B. D.; Schaefer, W. P.; Bercaw, J. E. *J. Am. Chem. Soc.* **1987**, *109*, 203–219. (d) Evans, W. J.; Chamberlain, L. R.; Ulibarri, T. A.; Ziller, J. W. *Ibid.* **1988**, *110*, 6423–6432. (e) den Haan, K. H.; Wielstra, Y.; Teuben, J. H. *Organometallics* **1987**, *6*, 2053–2060.
(27) (a) Jordan, R. F.; Guram, A. S. *Organometallics* **1990**, *9*, 2116–2123. (b) Erker, G.; Muhlenbernd, T.; Benn, R.; Rufiska, A. *Ibid.* **1986**, *5*, 402–404. (c) Fanwick, P. E.; Kobriger, L. M.; McMullen, A. K.; Rothwell, I. P. *J. Am. Chem. Soc.* **1986**, *108*, 8095–8097. (d) Evans, W. J.; Meadows, J. H.; Hunter, W. E.; Atwood, J. L. *Ibid.* **1984**, *106*, 1291–1300.
(28) (a) Cordone, R.; Taube, H. *J. Am. Chem. Soc.* **1987**, *109*, 8101–8102. (b) Cordone, R.; Harman, W. D.; Taube, H. *Ibid.* **1989**, *111*, 2896–2900.
(29) Covert, K. J.; Wolczanski, P. T. *Inorg. Chem.* **1989**, *28*, 4565–4567. Spectral (EPR, UV–vis) characterization and synthesis of (silox)$_3$Ti (**2**) are included in this communication. A manuscript detailing the study of this complex and its one-electron chemistry, including a free-radical ring opening of THF, is in preparation.
(30) For a phenoxide analogue, (2,6-^{t}Bu-C$_6$H$_3$O)$_3$Ti, see: Latesky, S. J.; Keddington, J.; McMullen, A. K.; Rothwell, I. P.; Huffman, J. C. *Inorg. Chem.* **1985**, *24*, 995–1001.

$[(Me_3Si)_2N]_3Sc$[31] to 3 equiv of H(silox) in hydrocarbon solvents resulted in a complex mixture due to degradation of the amides. When the silanolysis was conducted with 5 equiv of H(silox), colorless crystals of $(silox)_3ScNH_3$ (**3**-NH_3) were isolated in 65% yield according to eq 2. Characteristic IR absorptions at 3371 and 3281 cm^{-1} were diagnostic for the ammonia ligand. Although the mechanism of silanolysis is unknown, $N(p\pi) \rightarrow Sc(d\pi)$ donation probably renders the amide silicon susceptible to nucleophilic attack, even by a large nucleophile, $^tBu_3SiOH$. Attack by (silox)H on free $(Me_3Si)_2NH$ was not observed. Removal of either THF or NH_3 from the Lewis acidic scandium centers of **3**-THF and **3**-NH_3 proved difficult to execute, despite exhaustive attempts at various thermolytic procedures (e.g., 10^{-4} Torr, 190 °C).

For comparison to $(silox)_3Ta$ (**1**), the first-row d^2 vanadium analogue was sought. Treatment of VCl_3 with 3 equiv of Na(silox) in THF afforded aqua blue $(silox)_3V(THF)$ (**4**-THF, eq 3) in 51%

$$VCl_3 + 3Na(silox) \xrightarrow[70\ °C,\ 12\ h,\ -3NaCl]{THF,\ 25\ °C,\ 17\ h} \underset{4\text{-THF}}{(silox)_3V(THF)} \quad (3)$$

yield upon crystallization from toluene. Vacuum thermolysis of **4**-THF at 150 °C for 48 h failed to remove the THF, and since reactivity studies indicated that it was labile,[32] no further attempts were undertaken. Unlike base-free **1**, **4**-THF is paramagnetic ($d_{xz}^1 d_{yz}^1$), with a broad silox resonance at δ 1.6 ($\nu_{1/2} \sim 250$ Hz) in the ^1H NMR (C_6D_6) spectrum and an effective magnetic moment (μ = 3.7 μ_B 25 °C)[33] indicative of contributions from spin–orbit coupling and second-order Zeeman effects.[34]

Unsaturated Hydrocarbon Adducts of $(silox)_3M$. Previously,[22] $(silox)_3Ta$ (**1**) was shown to react rapidly (<5 min) with excess ethylene or propylene to produce yellow-orange $(silox)_3Ta(\eta\text{-}C_2H_4)$ (**5a**) and orange-red $(silox)_3Ta(\eta\text{-}C_2H_3Me)$ (**5b**; eq 4). The alkene

$$\underset{1}{(silox)_3Ta} + RHC{=}CHR' \xrightarrow[\text{hexanes or benzene}]{25°C} (silox)_3Ta(\eta\text{-}RHC{=}CHR') \quad (4)$$

R' = H, R = H, **5a**; Me, **5b**; Et, **5c**
R = R' = Me, **5d**

complexes, illustrated as metallacyclopropanes because of the reduction capability of the Ta(III) center,[35,36] were crystallized from hexanes in 63% and 56% yield, respectively. In sealed NMR tube experiments, an orange-red solution of $(silox)_3Ta(\eta\text{-}C_2H_3Et)$ (**5c**) formed when **1** was treated with 1 equiv of 1-butene. Similarly, $(silox)_3Ta$ (**1**) was exposed to 1 equiv of *cis*- and *trans*-2-butene in benzene-d_6. While the former reacted over the course of 3 days to generate $(silox)_3Ta(\eta\text{-}cis\text{-}HMeC{=}CHMe)$ (**5d**), no equilibrium binding of *trans*-2-butene to the tantalum center was detected; 3,3-dimethyl-1-butene and tetramethylethylene were also unreactive toward **1**. Isolation of **5c** and **5d** was complicated by competition from cyclometalation of the silox group (vide infra). Evidence for the complexation of additional olefin equivalents in

Scheme I

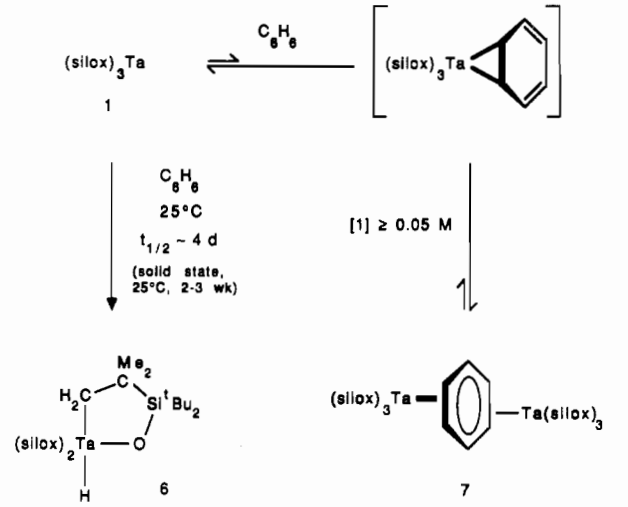

the form of adducts or metallacyclopentanes or as dimerization products (e.g., 1-butene, etc.) was not detected. In **5a–d**, ^1H and $^{13}C\{^1H\}$ NMR studies revealed equivalent silox groups, consistent with a relatively low barrier to rotation about the cylindrically symmetric axis present in pyramidal $(silox)_3M$.[37]

A qualitative comparison of the rates of olefin complexation, based on 1:1 stoichiometry at 25 °C, appears to reflect the relative steric requirements of the R groups. Under these conditions, the ethylene adduct formed slightly faster (<10 min) than the propylene complex, but 19 h were required for the maximum formation of **5c**, and **5d** was generated over a 2–3-day period. A preference for binding *cis*- vs *trans*-olefins is typical,[1] but the disparity in this case is conspicuous. Figure 1 shows three probable ground state conformations for 1-alkene (I) and *cis*- (II) and *trans*-olefin (III) complexes. Any ground state structure of a *trans*-olefin complex will exhibit one roughly eclipsed silox/R interaction, whereas the substituents in either I or *cis*-olefin adduct II can be situated to give conformers bereft of such energetically unfavorable influences. Therefore, it is plausible that *trans*-2-butene, 3,3-dimethyl-1-butene, and tetramethylethylene complexes are kinetically viable, yet thermodynamically unstable with respect to the free olefin and **1**. Similar steric interactions should be operative in the transition state for olefin complexation. Since alkyl substituents raise the levels of the π and π^* orbitals,[1,37] the observed trend is also consistent with the dominance of π-backbonding, provided the transition state is influenced by the same electronic factors that affect alkene binding.

Cyclometalation[38] of $(silox)_3Ta$ (**1**) occurred slowly ($t_{1/2} \sim 4$ days) at 25 °C (~12 h at 70 °C) in benzene to provide $(silox)_2HTaOSi^tBu_2CMe_2CH_2$ (**6**; Scheme I),[22,39] thereby competing with the complexation of substituted olefins. It is conceivable that the *trans*-2-butene, 3,3-dimethyl-1-butene and C_2Me_4 complexes of **1** are thermodynamically viable, yet kinetically uncompetitive with respect to cyclometalation. Light blue crystalline **1** transformed into a white powder after 2–3 weeks at 25 °C; crystallization from THF afforded colorless, waxy **6** in 84% yield. The spectral data are consistent with a trigonal bipyramid com-

(31) (a) $[(Me_3Si)_2N]_3Sc$: Ghotra, J. S.; Hursthouse, M. B.; Welch, A. J. *J. Chem. Soc., Chem. Commun.* **1973**, 669–670. (b) Sc(2,6-^{t}Bu,4-Me-$C_6H_2O)_3$: Hitchcock, P. B.; Lappert, M. G.; Singh, A. *Ibid.* **1983**, 1499–1501.

(32) (a) A brief report of $(RO)_3V$ (R = Ph_3Si, Et_3C) has appeared. See: Horvath, B.; Strutz, J.; Geryer-Lippmann, J.; Horvath, E. G. *Z. Anorg. Allg. Chem.* **1981**, *483*, 181–192. (b) For related V(III) compounds, see: Feher, F. J.; Walzer, J. F. *Inorg. Chem.* **1990**, *29*, 1604–1611.

(33) (a) Deutsch, J. L.; Poling, S. M. *J. Chem. Educ.* **1969**, *46*, 167–168. (b) Evans, D. F. *J. Chem. Soc.* **1959**, 2003–2005.

(34) (a) Drago, R. S. *Physical Methods in Chemistry*; W. B. Saunders: Philadelphia, PA, 1977. (b) Hellwege, K.-H., Hellwege, A. M., Eds.; *Magnetic Properties of Coordination and Organometallic Transition Metal Compounds, Landolt-Bornstein Series*; Springer-Verlag: Berlin, 1981; Vol. 11 and references therein.

(35) (a) Sneeden, R. P. A. *Comprehensive Organometallic Chemistry*; Wilkinson, G., Stone, F. G. A., Abel, E. W., Eds.; Pergamon: New York, 1982; Vol. 3. (b) Ittel, S. D.; Ibers, J. A. *Adv. Organomet. Chem.* **1976**, *14*, 33–56.

(36) (a) Schultz, A. J.; Brown, R. K.; Williams, J. M.; Schrock, R. R. *J. Am. Chem. Soc.* **1981**, *103*, 169–176. (b) Cohen, S. A.; Auburn, P. R.; Bercaw, J. E. *Ibid.* **1983**, *105*, 1136–1143.

(37) Albright, T. A.; Hoffmann, R.; Thibeault, J. C.; Thorn, D. L. *J. Am. Chem. Soc.* **1979**, *101*, 3801–3812.

(38) For general references on cyclometalation in early-transition-metal systems, see: (a) Rothwell, I. P. *Polyhedron* **1985**, *4*, 177–200. (b) Rothwell, I. P. *Acc. Chem. Res.* **1988**, *21*, 153–159.

(39) Attempts to measure the cyclometalation rate of $(silox)_3Ta$ (**1**) to $(silox)_2HTaOSi^tBu_2CMe_2CH_2$ (**6**) have been hampered by complications. The presence of unidentified minor byproducts has interfered with ^1H NMR monitoring, and kinetics obtained by following the disappearance of **1** (612 nm) in cyclohexane by UV–vis spectroscopy have suffered problems due to the low concentrations required and the high air sensitivity of **1**. The most reproducible data indicate that $-d[\mathbf{1}]/dt = k_{obs}[\mathbf{1}]$ (k_{obs} = 4.8 (1) × 10^{-4} s^{-1}, 0.029 M, 75 °C; 2.1 (1) × 10^{-4} s^{-1}, 0.029 M, 0.044 M, 64.4 °C; 1.0 (1) × 10^{-4} s^{-1}, 0.059 M, 56.4 °C). Harpp, K. S.; Wolczanski, P. T. Unpublished results.

prising an axial hydride (δ 21.97, TaH; ν(TaH) = 1770 cm^{-1}) and alkyl (i.e., Scheme I),[40] or one in which the metallacycle oxygen and the hydride are trans-axial. The former is preferred since the π-donating oxygen is in the equatorial plane;[41] furthermore, this configuration minimizes long-range steric interactions of the ^{t}Bu groups in the silox and cyclometalated ligands.

When a solution was allowed to stand for 10–14 days in a concentrated benzene solution (~0.10 M), (silox)$_3$Ta (**1**) deposited dark brown crystals of [(silox)$_3$Ta]$_2$\{μ-η^2(1,2):η^2(4,5)-C$_6$H$_6$\} (**7**; ~7%) while cyclometalating to **6** (Scheme I). Extended hydrolysis of [(silox)$_3$Ta]$_2$\{μ-η^2(1,2):η^2(4,5)-C$_6$H$_6$\} (**7**) in THF-d_8 (sealed tube, 3 days, ~100 °C) produced a fine white precipitate (probably Ta$_2$O$_5$), C$_6$H$_6$, and (silox)H (^{1}H NMR); dihydrogen is also presumed to form, but was not detected. The relatively drastic hydrolysis conditions suggest that penetration of the hydrocarbon periphery of **7** by a polar reagent such as water must be extremely difficult. The structure of **7** has been corroborated via single-crystal X-ray diffraction studies,[24] but the bridging group was not well resolved and its exact geometry is somewhat ambiguous. The data are most consistent with the η^2(1,2):η^2(4,5) description, but the possibility of a bis-η^3 arrangement[42,43] cannot be completely dismissed given a slightly asymmetric binding of the μ-C$_6$H$_6$ bridge. Magnetic measurements on a Faraday balance revealed that **7** was diamagnetic, and EHMO calculations manifested a substantial HOMO–LUMO gap derived from extensive orbital mixing in C_i symmetry.[44]

As the scheme illustrates, the formation of **7** at high concentrations of **1** is consistent with a preequilibrium involving monoadduct (silox)$_3$Ta(C$_6$H$_6$), a molecule of unknown hapticity, followed by trapping by **1**. According to this interpretation, the formation of **7** would be second-order in [**1**] as opposed to the first-order cyclometalation process (**1** → **6**),[39] thus providing a rationale for the concentration dependence. When **1** was exposed to neat *p*-xylene, only the cyclometalated product (**6**) was observed. In an attempt to isolate a mononuclear π-arene species as a model for the putative intermediate, **1** was treated with naphthalene, since less aromatic stabilization must be overcome for complexation of C$_{10}$H$_8$.[3,45–47] Even in the presence of excess C$_{10}$H$_8$, **6** was the only observed product. Presumably, coordination at the 2- and 3-positions would require loss of aromaticity in the second ring and attack at the 1- and 2-positions would cause unfavorable steric interactions.

In THF-d_8, the ^{1}H NMR spectrum of [(silox)$_3$Ta]$_2$\{μ-η^2(1,2):η^2(4,5)-C$_6$H$_6$\} (**7**) showed two very weak resonances at δ 1.20 and 4.80 that were tentatively assigned as the silox and benzene ligands, respectively. When prepared from C$_6$D$_6$ (**7**-d_6), the resonance at δ 4.80 was absent. In benzene-d_6, brown **7** did not appear to undergo ligand exchange with the solvent, even at 100 °C, but since no solvent discoloration was observed, its solubility was suspect. The ^{13}C NMR (THF-d_8) exhibited weak resonances at δ 85.21 (μ-C$_6$H$_6$), 31.53 (C(*C*H$_3$)$_3$), and 24.17 (*C*(CH$_3$)$_3$), but the assignments are again tenuous due to the insolubility of **7**. The resonances attributed to the benzene ligand compare well with the reported values for other benzene complexes: (CpVH)$_2$(C$_6$H$_6$), ^{1}H δ 3.99, ^{13}C δ 76.2;[5] [Cp*Re(CO)$_2$]$_2$[μ-η^2(1,2):η^2(3,4)-(C$_6$H$_6$)], ^{1}H δ 2.85, 4.14, 6.41, ^{13}C δ 40.9, 50.6, 127.3;[13] [Os(NH$_3$)$_5$]$_2$[μ-η^2(1,2):η^2(3,4)-(C$_6$H$_6$)]$^{4+}$, ^{1}H δ 4.33, 4.63, 6.45, ^{13}C δ 49.6, 53.1, 127.6.[10]

Acetylene reacted rapidly (~30 min) with **1** at 25 °C to form colorless (silox)$_3$Ta(η-C$_2$H$_2$) (**8a**) in 72% isolated yield (eq 5). The

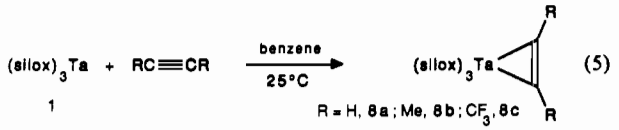

(5)

acetylene hydrogens appeared at δ 11.91 in the ^{1}H NMR spectrum, in good agreement with other unsubstituted early metal acetylenes,[48,49] and the downfield acetylenic resonance (δ 216.97, J_{CH} = 169 Hz) in the ^{13}C\{^{1}H\} NMR spectrum characterized a four-electron donor.[50] When 2-butyne was added to **1**, the reaction proceeded more slowly ($t_{1/2}$ ~ 9 h, 25 °C) to give (silox)$_3$Ta(η-MeCCMe) (**8b**; eq 7),[22] in part due to the greater bulk of this alkyne. In a sealed NMR tube experiment, 1.0 equiv of hexafluoro-2-butyne reacted instantly with **1** upon thawing of the C$_6$D$_6$ to generate (silox)$_3$Ta(η^2-F$_3$CC$_2$CF$_3$) (**8c**). Since F$_3$CC≡CCF$_3$ is larger than MeC≡CMe and HC≡CH, the qualitative rate differences appear to reflect the same electronic influences that effect the ground state. Both the π^b and π^* orbitals of F$_3$CC≡CCF$_3$ are significantly lowered relative to RC≡CR, resulting in weaker CC(π^b) → Ta(dσ) and stronger Ta(dπ) → CC(π^*) interactions, thus confirming the metallacyclopropene depiction.[1,49–51]

Unlike (silox)$_3$Ta (**1**), the titanium, vanadium, and scandium analogues did not form simple adducts with ethylene or 2-butyne. Exposure to **2** to 0.5 equiv of ethylene resulted in the near-quantitative formation of a yellow precipitate, tentatively formulated as [(silox)$_3$Ti]$_2$(μ-C$_2$H$_4$) (**9**; eq 6) on the basis of stoi-

$$\underset{\mathbf{2}}{(\text{silox})_3\text{Ti}} + 0.5\text{C}_2\text{H}_4 \xrightarrow[\text{hexane}]{25\ ^\circ\text{C}} \underset{\mathbf{9}}{[(\text{silox})_3\text{Ti}]_2(\mu\text{-C}_2\text{H}_4)} \quad (6)$$

chiometric, analytical, and IR evidence. Unfortunately, **9** proved insoluble in hydrocarbon and ethereal solvents, and attempts to quench the binuclear complex with H$_2$O/THF were ineffective, even at elevated temperatures. Difficult H$_2$O/THF quenches have been encountered in the cases of [(silox)$_3$Ta]$_2$\{μ-η^2(1,2):η^2-(4,5)-C$_6$H$_6$\} (**7**) and [(silox)$_3$Ta]$_2$(μ-C$_2$).[23] Apparently, if a bridging group such as μ:η^1,η^1-C$_2$H$_2$ can bring two (silox)$_3$M centers very close, the ^{t}Bu groups of the ligands may virtually interlock. The molecule then resembles a hydrocarbon sphere that is difficult to solvate and almost impenetrable to hydrolytic or other polar media. Since the yellow color is indicative of Ti(IV), the most likely structure is (silox)$_3$Ti–CH$_2$CH$_2$–Ti(silox)$_3$, one in which the Ti(III) centers have added to the ethylene in one-electron steps.[52,53]

As expected, ethylene does not effectively compete with the bound THF or NH$_3$ of d^0 (silox)$_3$ScL (L = THF, **3**-THF; NH$_3$, **3**-NH$_3$). Ethylene and F$_3$CC≡CCF$_3$ were similarly unreactive toward (silox)$_3$V(THF)(**4**-THF), as was 2-butyne at 25 °C, but decomposition occurred after 3 days at 100 °C, resulting in free ^{t}Bu$_3$SiOH and an uncharacterized black precipitate. The paramagnetic, first-row V(III) complex (**4**-THF) prefers the σ-donor THF instead of the softer alkene or alkyne in contrast to its

(40) Similar shifts are observed for tbp (silox)$_3$TaH$_2$ (δ 21.99)[23] and (silox)$_3$TaH(C$_2$H$_5$) (δ 22.30): LaPointe, R. E.; Wolczanski, P. T. *J. Am. Chem. Soc.* **1986**, *108*, 3535–3537.
(41) Rossi, A. R.; Hoffmann, R. *Inorg. Chem.* **1975**, *14*, 365–374.
(42) Keasey, A.; Bailey, P. M.; Maitlis, P. M. *J. Chem. Soc., Chem. Commun.* **1978**, 142–143.
(43) (a) Jonas, K.; Koepe, G.; Schieferstein, L.; Mynott, R.; Krüger, C.; Tsay, Y.-H. *Angew. Chem., Int. Ed. Engl.* **1983**, *22*, 620–621. (b) Jonas, K.; Koepe, G.; Schieferstein, L.; Mynott, R.; Krüger, C.; Tsay, Y.-H. *Angew. Chem., Suppl.* **1983**, 920–928.
(44) Zonnevylle, M. C. Ph.D. Thesis, Cornell University, Ithaca, NY, 1989.
(45) Jonas, K. *J. Organomet. Chem.* **1974**, *78*, 273–279.
(46) Brauer, D. J.; Krüger, C. *Inorg. Chem.* **1977**, *16*, 884–891.
(47) Albright, J. O.; Datta, S.; Dezube, B.; Kouba, J. K.; Marynick, D. S.; Wreford, S. S.; Foxman, B. M. *J. Am. Chem. Soc.* **1979**, *101*, 611–619.
(48) (a) Alt, H. G. *J. Organomet. Chem.* **1977**, *127*, 349–356. (b) Serrano, R.; Royo, P. *Ibid.* **1983**, *247*, 33–37. (c) Lewis, L. N.; Caulton, K. G. *Ibid.* **1983**, *252*, 57–69.
(49) Hoffman, D. M.; Hoffmann, R.; Fisel, C. R. *J. Am. Chem. Soc.* **1982**, *104*, 3858–3875.
(50) (a) Templeton, J. L.; Ward, B. C. *J. Am. Chem. Soc.* **1980**, *102*, 3288–3290. (b) Templeton, J. L. *Adv. Organomet. Chem.* **1989**, *29*, 1–100.
(51) (a) Chao, Y. W.; Wexler, P. A.; Wigley, D. E. *Inorg. Chem.* **1989**, *28*, 3860–3868. (b) Theopold, K. H.; Holmes, S. J.; Schrock, R. R. *Angew. Chem., Int. Ed. Engl.* **1983**, *22*, 1010–1011. (c) Cotton, F. A.; Hall, W. T. *Inorg. Chem.* **1980**, *19*, 2352–2354. (d) Smith, G.; Schrock, R. R.; Churchill, M. R.; Youngs, W. J. *Ibid.* **1981**, *20*, 387–393.
(52) (a) Wengrovius, J. H.; Schrock, R. R.; Day, C. S.; Inorg. *Chem.* **1981**, *20*, 1844–1849. (b) Cotton, F. A.; Kibala, P. A. *Polyhedron* **1987**, *6*, 645–646. (c) Kaminsky, W.; Kopf, J.; Sinn, H.; Vollmer, H.-J. *Angew. Chem., Int. Ed. Engl.* **1976**, *15*, 629–630.
(53) For related MCH$_2$CH$_2$M′ complexes, see: (a) Bullock, R. M.; Lemke, F. R.; Szalda, D. J. *J. Am. Chem. Soc.* **1990**, *112*, 3244–3245. (b) Beck, W. *Polyhedron* **1988**, *7*, 2255–2261.

Table I. ^{1}H NMR Spectral Data for (silox)$_3$Ta(η^2-NCR(CH)$_3$CR′-*N,C*) (R = R′ = H, **10a**; R = H, R = Me, **10b**; R = R′ = Me, **11b**), (silox)$_3$Ta(η^2-1,2-$N_2C_4H_4$) (**12**), and (silox)$_3$Ta(η^2-1,3-$N_2C_4H_4$) (**13**) Derivatives (*Ta = (silox)$_3$Ta)[a]

positions	pyridine[b]	**10a**[c]	**10b**	**11b**	**12**	**13**
2	8.53, "t"	3.89, br s	4.39, br s	...	...	3.66, s
3	6.67, "m"	6.44, d"t"d $J_{3,4}$ = 9.3 J = 1.6, <0.5	6.61, d $J_{3,4}$ = 9.3	6.38, d $J_{3,4}$ = 9.2	9.54, t $J_{3,4}$ = 2.6	6.19, d"m" $J_{3,4}$ = 6.7
4	7.00, "tt"	5.73, dddd $J_{3,4}$ = 9.3 $J_{4,5}$ = 5.7 J = 1.7, 1.0	5.82, ddd $J_{3,4}$ = 9.3 $J_{4,5}$ = 5.7 $J_{2,4}$ = 1.5	5.93, dd $J_{3,4}$ = 9.3 $J_{4,5}$ = 5.7	6.02, t $J_{3,4}$ = 2.6	6.68, dd $J_{3,4}$ = 6.7 $J_{4,6}$ = 1.6
5	6.67, "m"	5.22, "t" $J_{4,5}$ = 5.7 $J_{5,6}$ = 6.2	5.25, d $J_{4,5}$ = 5.7	5.36, d $J_{4,5}$ = 5.7	...	...
6	8.53, "m"	7.40, d"m" $J_{5,6}$ = 6.2	...	...	...	8.40 $J_{4,6}$ = 1.6
Me	...	...	2.21	2.18, 1.92	...	...
silox	...	1.21	1.26	1.27	1.33	1.20

[a] Chemical shifts are reported in δ relative to TMS (δ 0.0) or benzene-d_6 (δ 7.15); coupling constants are given in Hz. [b] Reference 54. [c] Toluene-d_8. For spectral data pertaining to pyridazine (1,2-$N_2C_4H_4$) and pyrimidine (1,3-$N_2C_4H_4$), see refs 63 and 64, respectively.

Table II. ^{13}C or ^{13}C{^{1}H} NMR Spectral Data for (silox)$_3$Ta(η^2-NCR(CH)$_3$CR′-*N,C*) (R = R′ = H, **10a**; R = H, R′ = Me, **10b**; R = R′ = Me, **11b**), (silox)$_3$Ta(η^2-1,2-$N_2C_4H_4$) (**12**), and (silox)$_3$Ta(η^2-1,3-$N_2C_4H_4$) (**13**) Derivatives (*Ta = (silox)$_3$Ta)[a]

positions	pyridine[b]	**10a**[c]	**10b**[c]	**11b**[d]	**12**[d]	**13**[d]
2	150.2 (178)	81.96 (157)	87.14	92.68		80.79
3	123.9 (162)	128.24 (158)	124.94	125.70	156.29 (169)	118.27
4	135.9 (162)	121.30 (158)	121.72	122.40	138.54 (157)	133.64
5	123.9 (162)	109.69 (160)	108.59	108.38		
6	150.2 (178)	144.75 (175)	139.80	124.53		158.68
Me			30.54	31.75[e]		
silox		23.94, 31.05	23.54, 30.93	23.96, 31.07	23.44, 31.10	23.50, 30.60

[a] Chemical shifts are reported in δ relative to TMS (0.0) with $^1J_{CH}$ (Hz) in parentheses. [b] Reference 54. [c] Cyclohexane-d_{12}. [d] Benzene-d_6. [e] Second Me group was not located and assumed to be obscured by silox resonance. For spectral data pertaining to pyridazine (1,2-$N_2C_4H_4$) and pyrimidine (1,3-$N_2C_4H_4$), see refs 63 and 64, respectively.

third-row congener, (silox)$_3$Ta (**1**), an observation rationalized by EHMO calculations.

Heterocyclic π-Complexes of (silox)$_3$Ta (1). Treatment of (silox)$_3$Ta (**1**) with pyridine, 1.0 equiv or an excess, resulted in an orange solution from which amber crystals of (silox)$_3$Ta(η^2-NC_5H_5-*N,C*) (**10a**) could be isolated in 65% yield (eq 7).[24]

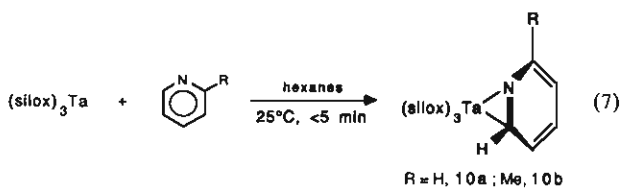

(7)

R = H, **10a**; Me, **10b**

^{1}H and ^{13}C NMR spectra revealed five inequivalent ring positions (Tables I and II), indicating an η^2-bound pyridine ligand. The α-^{13}C and α-^{1}H resonances in free pyridine are found at δ 150.2 (J_{CH} = 178 Hz) and 8.53, respectively.[54] Upon complexation, one set of α resonances dropped dramatically to δ 81.96 and 3.89 with J_{CH} = 157 Hz, signifying an increased amount of p character in the bound carbon, while the other set exhibited minor changes (δ 144.75 and 7.40 with J_{CH} = 175 Hz). Extensive coupling between all protons except the broad singlet at δ 3.89 imply an η^2-C,N coordination, with H(2) distorted out of the NC_5H_5 plane and away from the tantalum due to pyramidalization at C(2).

Verification of the "side-on", η^2-N,C binding of the pyridine was accomplished via X-ray crystallography, as summarized by the skeletal view in Figure 2.[24] The structure of diene-like

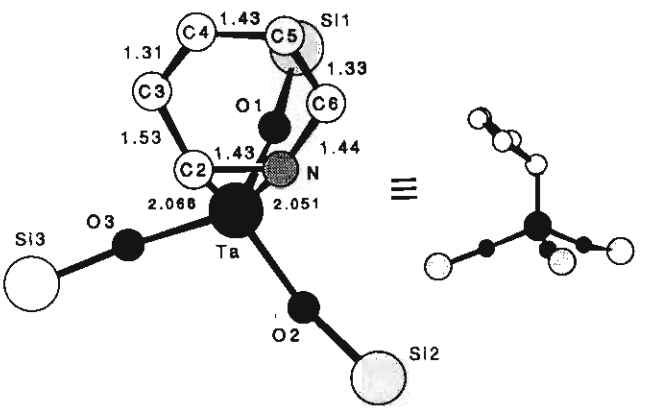

Figure 2. Skeletal view of (silox)$_3$Ta(η^2-NC_5H_5-*N,C*) (**10a**).

(silox)$_3$Ta(η^2-NC_5H_5-*N,C*) (**10a**) is indicative of a tantalum(V) metallaaziridine,[55-57] where the aromaticity of the pyridine has been interrupted by strong Ta(dπ) → py(π^*) back-bonding. The NC_5 ring of (DIPP)$_2$ClTa(η^2-2,4,6-NC_5H_2^{t}Bu$_3$-*N,C*), recently

(54) Katritsky, A. R.; Rees, C. W.; Boulton, A. J.; McKillop, A. *Comprehensive Heterocyclic Chemistry*; Pergamon Press: New York, 1984; Vol. 2.

(55) Durfee, L. D.; Fanwick, P. E.; Rothwell, I. P.; Folting, K.; Huffman, J. C. *J. Am. Chem. Soc.* **1987**, *109*, 4720–4722 and references therein.

(56) Durfee, L. D.; Hill, J. E.; Kerschner, J. L.; Fanwick, P. E.; Rothwell, I. P. *Inorg. Chem.* **1989**, *28*, 3095–3096.

(57) (a) Chamberlain, L. R.; Rothwell, I. P.; Huffman, J. C. *J. Chem. Soc., Chem. Commun.* **1986**, 1203–1204. (b) Mayer, J. M.; Curtis, C. J.; Bercaw, J. E. *J. Am. Chem. Soc.* **1983**, *105*, 2651–2660. (c) Chiu, K. W.; Jones, R. A.; Wilkinson, G.; Galas, A. M. R.; Hursthouse, M. B. *J. Chem. Soc., Dalton Trans.* **1981**, 2088–2097. (d) Wolczanski, P. T.; Bercaw, J. E. *J. Am. Chem. Soc.* **1979**, *10*, 6450–6452 and references therein.

prepared by Wigley et al.,[25] is severely distorted, presumably because of ^{t}Bu steric interactions. In Taube's $[(H_3N)_5Os(\eta^2$-2,6-$NC_5H_3Me_2$-$C,C')]^{2+}$ dication, the lutidine is η^2-bound, but through the carbons in the 3- and 4-positions.[28] EHMO calculations performed on $(HO)_3Ta(\eta^2$-NC_5H_5-$N,C)$ (**10a'**) corroborate the observed η^2-N,C binding.

NMR spectra of **10a** were assigned in accord with decoupling, HETCOR, and α-D labeling studies, and the shifts of similar complexes (Tables I and II) were correlated to these data. Exposure of (silox)$_3$Ta (**1**) to 2-picoline provided (silox)$_3$Ta(η^2-6-NC_5H_4Me-N,C) (**10b**) in 62% yield according to eq 7. Since the resonance analogous to H(6) in **10a** was absent in the spectrum of **10b**, its methyl group was located exclusively in the more sterically favorable 6-position. The remaining protons displayed minor downfield shifts from the parent compound (**10a**), perhaps indicative of slightly weaker bonding of the substituted pyridine. The largest shift (0.5 ppm) was observed for H(2), consistent with a more sp^2-like carbon resulting from a weakened interaction of the Me-substituted substrate with the (silox)$_3$Ta core.

Rehybridization of C(2), leading to an sp^3 carbon center in **10a,b** should direct H(2) out of the plane of the pyridine ring and away from tantalum, consistent with the aforementioned spectral data. The η^2-py-N,C binding mode forces the α-H proximate to Ta, probably within 2.3 Å (attempts to locate H(2) in the crystallographic refinement were unsuccessful); therefore, an agostic interaction[58] placing H(2) closer to the electrophilic tantalum center could also account for the observed chemical shifts and coupling constants. The possibility of an agostic interaction was probed by generating the α-deuterio-pyridine[59] complex (**10a**-d_1) under equilibrating conditions (vide infra) and looking for an equilibrium isotope effect,[60,61] since IR spectra provided no evidence of its existence. The heavier deuterium isotope should show a preference for the more strongly bound position, C(6), rather than the possible agostic position, C(2). With both ^{1}H and ^{2}H NMR, 50 (±3)% D incorporation was observed in both positions; hence, a *significant* isotope effect was not observed.[60] EHMO calculations performed on $(HO)_3Ta(\eta^2$-NC_5H_5-$N,C)$ (**10a'**) favored pyramidalization at C(2); hence, the presence of an agostic interaction was discounted.

A nondissociative or dissociative pathway converting the η^2-py-N,C to a σ-N donor would symmetrize the pyridine, but variable-temperature ^{1}H NMR experiments with (silox)$_3$Ta(η^2-NC_5H_5-N,C) (**10a**) failed to detect such a process. Substitution with free pyridine did occur, albeit slowly, as evidenced by exchange with pyridine-d_5 (eqs 8 and 9). In view of a previously observed THF exchange on a related, sterically similar d^0 molecule, (^{t}BuSiNH)$_2$(^{t}BuSiN)Zr(THF), an associative substitution pathway was expected.[62] However, at 53.7 °C, under pseudo-first-order conditions (40–100 equiv of NC_5D_5), a zero-order dependence on pyridine was observed (k_{obs} = 1.3 (2) × 10^{-2} s^{-1}), consistent with dissociative substitution.

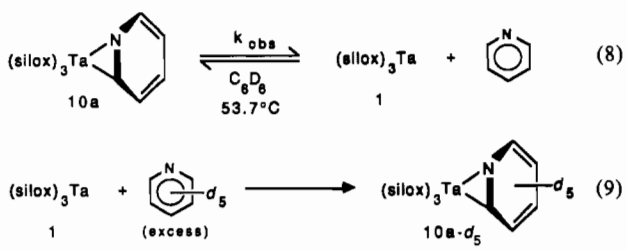

(8)

(9)

In order to test the steric requirements of η^2-N,C binding, (silox)$_3$Ta (**1**) was treated with one equiv of 2,6-lutidine in C_6D_6. The blue color faded in ~20 min at 25 °C, and the ^{1}H NMR (C_6D_6) spectrum showed an unexpected result; activation of the C–H bond in the 4-position cleanly occurred to give the 4-pyridyl–hydride species (silox)$_3$Ta(H)($C_5H_2Me_2N$) (**11a**; eq 10),

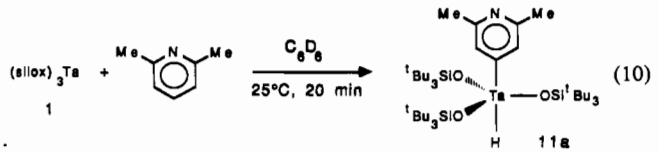

(10)

as evidenced by a singlet at δ 22.93, characteristic of a Ta–H unit,[39] and two singlets at δ 8.10 and 2.61 assigned as the ring hydrogens and α-methyl groups, respectively. The structure was corroborated by a ^{13}C NMR spectrum[63] that revealed resonances due to three ring carbons at δ 203.77 (4-C), 156.99 (2,6-C), and 130.04 (3,5-C) and a methyl resonance at δ 31.07 in addition to those attributed to silox. These shifts are comparable to those of a similar 2,6-lutidinium-4-yl species, $[(H_3N)_5Os(4$-$C_5H_2Me_2NH)]^{2+}$ (δ 210.2, 141.0, 136.8, and 19.2), prepared by Taube et al.[28] The inductive withdrawing effect of the ring nitrogen apparently guides the activation at the 4-CH position; EHMO calculations of **10a** support this premise.

When an NMR sample was allowed to stand for 3–4 days, the pyridyl–hydride **11a** slowly equilibrated with the side-bound lutidine isomer, (silox)$_3$Ta(η^2-2,6-$NC_5H_3Me_2$-N,C) (**11b**; eq 11),

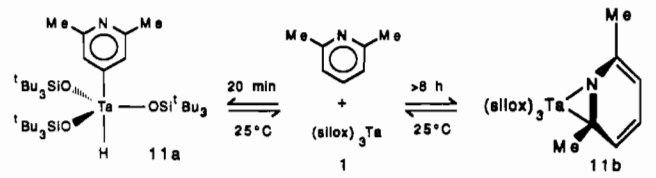

(11)

and an approximately equimolar mixture of 2,6-lutidine, **1**, **11a**, and **11b** was obtained in addition to some (silox)$_2$(H)TaOSi(^{t}Bu)$_2$CMe$_2$CH$_2$ (**6**). The η^2-N,C isomer (**11b**) was characterized by the presence of two methyl peaks and inequivalent ring protons in the ^{1}H NMR spectrum and confirmed by the appearance of the three methine and two quaternary carbons of the ring in the ^{13}C{^{1}H} spectrum (Tables I and II). If the equilibrium mixture was heated to 70 °C for 12 h, lutidine was released with complete formation of **6**. Sterics account for some of the reactivity delineated above. The Me substituents deter attack by **1** at the usual 1,2-N,C positions, and ground-state destabilization of **11b** permits observation of the equilibrium involving the pyridyl–hydride **11a**. Given the precedent set in the dissociative substitution of **10a**, the complexes probably equilibrate via reductive elimination of 2,6-lutidine from **11a** and dissociation from **11b**. Taube's $[(H_3N)_5Os(\eta^2$-2,6-$NC_5H_3Me_2$-$C,C')]^{2+}$ dication undergoes a similar, but irreversible and opposite rearrangement to the 2,6-lutidinium-4-yl species, $[(H_3N)_5Os(4$-$C_5H_2Me_2NH)]^{2+}$.

The unanticipated side-bound orientation of the pyridines prompted an investigation toward other heterocycles.[63,64] An

(58) (a) Brookhart, M.; Green, M. L. H.; Wung, L. H. *Prog. Inorg. Chem.* **1988**, *36*, 1–124. (b) Brookhart, M.; Green, M. L. H. *J. Organomet. Chem.* **1983**, *250*, 395–408.
(59) Abramovitch, R. A.; Kroeger, D. J.; Staskun, B. *Can. J. Chem.* **1962**, *40*, 2030–2032.
(60) Carpenter, B. K. *Determination of Organic Reaction Mechanisms*; John Wiley & Sons: New York, 1984; pp 83–111 and references therein.
(61) (a) Wolfsberg, M. *Acc. Chem. Res.* **1984**, *5*, 225–233. (b) Clawson, L.; Soto, J.; Buchwald, S. L.; Steigerwald, M. L.; Grubbs, R. H. *J. Am. Chem. Soc.* **1985**, *107*, 3377–3378. (c) Calvert, R. B.; Shapley, J. R. *Ibid.* **1978**, *100*, 7726–7727. (d) Calvert, R. B.; Shapley, J. R.; Schultz, A. J.; Williams, J. M.; Suib, S. L.; Stucky, G. D. *Ibid.* **1978**, *100*, 6240–6241.
(62) Cummins, C. C.; Schaller, C. P.; Van Duyne, G. D.; Wolczanski, P. T. Unpublished results.
(63) Castle, R. N., Ed. *Heterocyclic Compounds*; Wiley: New York, 1985; Vol. 28, 2,6-Lutidine: ^{1}H NMR (C_6D_6) δ 2.41 (Me_2, s, 6 H), 6.56 (m-CH, d, 2 H, J = 7.6 Hz), 7.01 (p-CH, t, 1 H, J = 7.6 Hz); ^{13}C{^{1}H} NMR (C_6D_6) δ 119.82 (p-C), 157.96 (o-C), 136.01 (m-C), 24.52 (Me). Pyridazine (1,2-$N_2C_4H_4$): ^{1}H NMR (C_6D_6) δ 6.21 (H(4), t, 2 H, J = 3.4 Hz), 8.66 (H(3), t, 2 H, J = 3.4 Hz); ^{13}C{^{1}H} NMR (C_6D_6) δ 125.31 (C(4), J_{CH} = 169 Hz), 151.48 (C(3), J_{CH} = 182 Hz).
(64) Weigert, F. J.; Husar, J.; Roberts, J. D. *J. Org. Chem.* **1973**, *38*, 1313. Pyrimidine (1,3-$N_2C_4H_4$): ^{1}H NMR (C_6D_6) δ 6.23 (H(3), t, 1 H, J = 5.0 Hz), 8.15 (H(2,4), d, 2 H, J = 5.2 Hz), 9.21 (H(6), s, 1 H); ^{13}C{^{1}H} NMR (C_6D_6) δ 121.28 (C(3), J_{CH} = 166 Hz), 156.65 (C(2,4), J_{CH} = 183 Hz), 159.54 (C(6), J_{CH} = 203 Hz).

interesting substrate proved to be pyridazine, 1,2-$N_2C_4H_4$,[63] which initially reacted with $(silox)_3Ta$ (**1**) to generate wine red $(silox)_3Ta(\eta^2\text{-}N_2C_4H_4\text{-}N,N')$ (**12**), according to ^1H and ^{13}C NMR

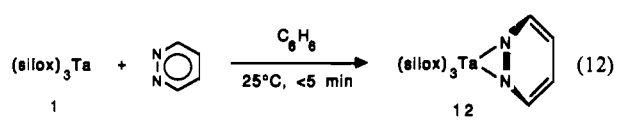

1 12 (12)

spectra that manifested its apparent C_s symmetry (Tables I and II). In reference to the previous examples, the pyridazine is preferentially illustrated as side-bound to the tantalum. The pyridazine adduct (**12**) was metastable, decomposing ($t_{1/2} \sim 1$ h) to unidentified product(s) whose ^1H NMR spectra were indicative of possible ring degradation.

When exposed to pyrimidine (1,3-$N_2C_4H_4$),[64] $(silox)_3Ta$ (**1**) bound the heterocycle at the 1,6-N,C junction to provide $(silox)_3Ta(\eta^2\text{-}1,3\text{-}N_2C_4H_4\text{-}N^1,C^6)$ (**13**). The ^1H and $^{13}C\{^1H\}$ NMR

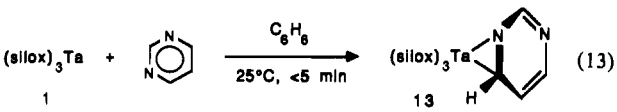

1 13 (13)

spectra of **13** were ambiguous in predicting the structure, since binding to either the 1,6-N,C or 1,2-N,C units would generate four distinct resonances. When **1** was treated with 1,3-$N_2C_4H_3D$-*2-d*)[65] to produce $(silox)_3Ta(\eta^2\text{-}1,3\text{-}N_2C_4H_3D\text{-}2\text{-}d\text{-}N^1,C^6)$ (**13-d**), the doublet at δ 8.40 was absent in the ^1H NMR spectrum, indicating that this position is not directly connected to the tantalum. Although pyridazine formed the anticipated adduct containing two Ta–N bonds (**12**), the pyrimidine compound (**13**) was unexpected in view of the potential 1,2-N,C site; the latter was favored because of the inductive effect of N(3) on the tantalum–carbon bond. EHMO calculations offer the rationale for the observed products. According to ^1H NMR spectra, the addition of pyrazine (1,4-$N_2C_4H_4$) to **1** appeared to generate $(silox)_3Ta(\eta^2\text{-}N_2C_4H_4\text{-}N,C)$, but the compound could not be purified, presumably due to disproportionation to $[(silox)_3Ta]_2(\eta^2\text{:}\eta^2\text{-}N_2C_4H_4\text{-}N,C\text{:}N,C)$, alternatively prepared from 2 equiv of **1** and pyrazine.

Pyridine Adducts of $(silox)_3M$ (M = Sc, Ti, V). The addition of 1.0 equiv or an excess of pyridine to d^0 $(silox)_3Sc(THF)$ (**3-THF**) produced colorless $(silox)_3Sc(py)$ (**3-py**) in 79% yield according to eq 14. Characterization of **3-py** through ^1H and

$$\begin{matrix}(silox)_3M(THF) \\ M = Sc\ (\textbf{3-THF}) \\ M = V(\textbf{4-THF})\end{matrix} + py \xrightarrow[25\ °C]{hexanes} \begin{matrix}(silox)_3Sc(py) + THF \\ M = Sc(\textbf{3-py}) \\ M = V\ (\textbf{4-py})\end{matrix} \quad (14)$$

$^{13}C\{^1H\}$ NMR and IR spectra indicated that the pyridine adopts the common σ-N-donor mode of binding,[20,21] as expected for a d^0 center. The d^2 $(silox)_3V(THF)$ (**4-THF**) complex also reacted with pyridine to generate a dark blue adduct, $(silox)_3V(py)$ (**4-py**) in 65% yield (eq 14). ^1H NMR spectra exhibited a broad resonance for the silox groups at δ 1.8 with $\nu_{1/2} \sim 350$ Hz, but signals corresponding to the bound pyridine were not located. Susceptibility measurements (μ = 3.7 μ_B, 25 °C) indicated a relatively high orbital contribution to the magnetic moment, as expected for a pseudotetrahedral d^2 species.[34] When combined with diagnostic IR spectra, the data strongly suggest that the pyridine is bound in the conventional η^1-mode.

EHMO calculations addressing various modes of pyridine binding to **2** were ambiguous, so there was hope that d^1 η^2-N,C complexes could be found. Treatment of **2** with 1.0 equiv or an excess of pyridine yielded monomeric, ink-blue $(silox)_3Ti(py)$ (**2-py**) in 63% yield (eq 15). The EPR spectrum of **2-py** (toluene

$$\underset{\textbf{2}}{(silox)_3Ti} + py \xrightarrow[25\ °C]{hexanes} \underset{\textbf{2-py}}{(silox)_3Ti(py)} \quad (15)$$

(65) For a preparation of (**2-d**, 1,3-$N_2C_4H_3D$), see: Hervieu, J.; Lautie-Mouneyrac, M.-F.; Dagant, J.; Dizabo, P.; Leiteh, L. C.; Renaud, R. N. *J. Labelled Compd.* **1972**, *8*, 365–379.

Table III. ^1H NMR Spectra (δ ($\nu_{1/2}$, Hz)) of $(silox)_3Ti(\eta^1\text{-py})$ (**2-py**) and Related 3,5-Lutidine (**2-3,5-**$NC_5H_3Me_2$), 4-Picoline (**2-4-**NC_5H_4Me), and 4-^{t}Bu-NC_5H_4 (**2-4-**$NC_5H_4{}^t$Bu) Derivatives[a]

positions	2-py	2-3,5-$NC_5H_3Me_2$	2-4-NC_5H_4Me	2-4-$NC_5H_4{}^t$Bu
2,6-H	−52.7 (420)	−52.7 (360)	−46.3 (330)	−47.1 (300)
3,5-H	27.5 (91)		23.2 (85)	24.2 (92)
4-H	−61.8 (450)	−59.4 (350)		
R		−17.9 (48)	64.1 (200)	2.7 (32)
silox	1.3 (38)	1.3 (30)	1.3 (34)	1.3 (35)

[a] Chemical shifts are reported relative to TMS (δ 0.0) or benzene-d_6 (δ 7.15).

glass, 77 K) revealed an axially symmetric pattern with broad, featureless absorptions at $g_\perp$ = 1.914 and $g_\parallel$ = 1.989 with g_{iso} = 1.939, indicative of a titanium localized electron. Presumably, the spectra manifest a static pyridine ligand (i.e., rhombic symmetry) in which the x and y axes cannot be distinguished.[66]

The titanium derivative (**2-py**) exhibited three diagnostic resonances in the ^1H NMR spectrum in addition to a broad silox resonance at δ 1.29 ($\nu_{1/2} \sim 13$ Hz), in accord with η^1-N-donor binding to a d^1 center (μ = 1.8 μ_B, 25 °C, Evans' method).[33] The 3,5-hydrogens resonated at δ 25 ($\nu_{1/2} \sim 65$ Hz), while the 2,6- and 4-hydrogens were in their characteristic upfield positions at δ −53 ($\nu_{1/2} \sim 600$ Hz) and δ −63 ($\nu_{1/2} \sim 400$ Hz), respectively.[67] Curie plots of δ vs $1/T$ for each site were linear from −90 to +60 °C, and each had a zero intercept, indicative of a simple paramagnet; no indication of fluxionality was observed.[67] From the magnitude of the contact shifts in **2-py**, it was possible to quantify the amount of unpaired spin density that is transferred to the π-system of the pyridine ligand. Upon application of the McConnell equation ($a_H = Q_{CH}\rho_C$, Q_{CH} = −23 G for aromatic carbons), the proton hyperfine (a_H) can be directly related to the spin density on the associated sp^2 carbon, ρ_C, and thus the spin density probabilities, ρ^2.[66-69] Utilizing $(silox)_3Sc(py)$ (**3-py**) as a diamagnetic reference, the contact shifts were used to derive the proton hyperfine couplings.[67] From the contact shifts and the McConnell equation the following data were obtained: 2,6-C, a_H = −0.822 G, ρ_C = 0.036, ρ^2 = 0.13%; 3,5-C, a_H = 0.280 G, ρ_C = −0.012, ρ^2 = 0.01%; 4-C, a_H = −0.914 G, ρ_C = 0.040, ρ^2 = 0.16%. As expected, the spin densities reflect the conjugative delocalization predicted from a simple valence-bond standpoint. Most of the spin density (>99%) is located on titanium and nitrogen atoms, consistent with the aforementioned EPR spectrum.

Other pyridine ligands surveyed via sealed NMR tube reactions displayed similar spectra indicative of η^1-ligation, as indicated in Table III. Dark blue adducts with 4-picoline (**2-4-**NC_5H_4Me), 4-*tert*-butylpyridine (**2-4-**$NC_5H_4{}^t$Bu), and 3,5-lutidine (**2-3,5-**$NC_5H_3Me_2$), prepared by adding ~1.0 equiv of the ligand to **2** in benzene-d_6 at 25 °C, helped confirm the above assignments. The 4-picoline derivative (**2-4-**NC_5H_4Me) was especially instructive, since the Me shift of δ 57 was opposite in sign from the 4-C of **2-py** at δ −63, indicative of substantial unpaired spin density localized in a pyridine π^*-orbital.[67] The magnitude of the contact shift of the Me group (~62 ppm vs that of the free ligand), leads to a calculated $a_H \sim 0.840$ G. Assuming the methyl substitution does not change the spin density at the 4-C, $Q(CCH_3)$ is calculated to be +21 G, well within the expected range. Unlike the aforementioned tantalum chemistry, 2,6-lutidine did not bind to **2**, and the ^1H NMR spectrum (25 °C) of a 1:1 mixture of **2** and 2-

(66) (a) Wertz, J. E.; Bolton, J. R. *Electron Spin Resonance*; Chapman and Hall: New York, 1986. (b) Ingram, D. J. E. *Free Radicals as Studied by Electron Spin Resonance*; Academic Press: New York, 1958. (c) Integration of the EPR spectrum of $(silox)_3Ti(py)$ (**2-py**) revealed no components upfield of $g_\parallel$ = 1.989. In combination with the line shape, the data is consistent with an axially symmetric system, or a rhombic system in which the x and y are similar.

(67) Eaton, D. R. In *NMR of Paramagnetic Molecules: Principles and Applications*; LaMar, G. N., Horrocks, W. D., Jr., Holm, R. H., Eds.; Academic Press: New York, 1973.

(68) McConnell, H. M.; Chestnut, D. B. *J. Chem. Phys.* **1958**, *28*, 107–117.

(69) For an example of this approach, see: Parks, J. E.; Holm, R. H. *Inorg. Chem.* **1968**, *7*, 1408–1416.

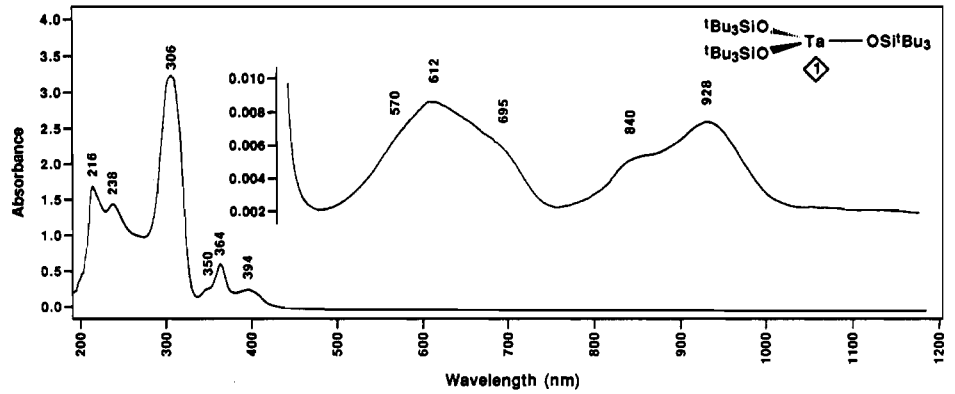

Figure 3. UV–vis spectrum of (silox)$_3$Ta (**1**).

picoline revealed an equilibrium with (silox)$_3$Ti(2-NC$_5$H$_4$Me) (**2**-2-NC$_5$H$_4$Me, eq 16). A rough estimate of the equilibrium

$$\underset{\mathbf{2}}{(\text{silox})_3\text{Ti}} + 2\text{-NC}_5\text{H}_4\text{Me} \underset{25\ ^\circ\text{C}}{\overset{\text{toluene}}{\rightleftharpoons}} \underset{\mathbf{2}\text{-2-NC}_5\text{H}_4\text{Me}}{(\text{silox})_3\text{Ti}(2\text{-NC}_5\text{H}_4\text{Me})} \quad (16)$$

constant (K_{eq}(20.0 (5) °C) = 18 (6) M^{-1}) was obtained by monitoring the chemical shift of the α-Me resonance of 2-picoline in the presence of various amounts of **2**.[70,71] Unfortunately, because the concentration of **2** could not be appreciably varied, the determination of K_{eq} was somewhat crude. Nonetheless, similar rough estimates were measured at different temperatures (toluene, 0.7–60.0 (5) °C) and application of the van't Hoff relation gave ΔH = −4.5 (2) kcal/mol and ΔS = −9.2 (7) eu.

Curiously, solution and Nujol mull IR spectra of **2**-py differed significantly from those of the Sc (**3**-py) and V (**4**-py) derivatives, which were nearly identical. The diagnostic pyridine ring band at ~1600 cm^{-1} is absent, and the remainder of the spectrum is of diminished intensity relative to those of **3**-py and **4**-py. Fortunately, the spectrum of **2**-py is also weaker and is overall dissimilar from that of (silox)$_3$Ta(η^2-NC$_5$H$_5$-*N*,*C*) (**10a**), which displays unmatched absorptions at 1596 and 1513 cm^{-1}. From these comparisons, the η^1-pyridine ligation so clearly observed in the NMR spectrum of **2**-py and related molecules may differ from that in **3**-py and **4**-py. In the latter two complexes, the transition metal is functioning as a simple Lewis acid, but in **2**-py, the ligand is partially reduced due to the reduction capability of the titanium(III) center (e.g., (silox)$_3$Ti^{IV}(py$^{\bullet-}$)). It is plausible that the spectra reflect this distinction. Partial reduction of bound pyridine ligands has been observed previously. Recent magnetic susceptibility and structural studies of Rothwell's tbp (2,6-^{i}Pr-OC$_6$H$_3$)$_2$Ti(py-4-Ph)$_3$ revealed significant bond length changes between the equatorial and axial pyridines, implicating reduction of the former (i.e., (2,6-^{i}Pr-OC$_6$H$_3$)$_2$(py-4-Ph)$_2$Ti^{III}(py-4-Ph$^{\bullet-}$)).[56] Despite the apparent partial reduction of the bound pyridine ligands, no evidence for coupling at the 4-position[55] or H-atom transfer reactions[72] has been obtained.

Discussion

UV–Vis Spectra of (silox)$_3$Ta (1). Inspection of the UV–vis spectrum of D_{3h} (silox)$_3$Ta (**1**) provides some insight into its character (Figure 3) and hence its unusual coordination geometry. The d^2 species (**1**) exhibits a rather complex spectrum dominated by intraligand (IL) and ligand-to-metal charge-transfer (LMCT) bands at 216 (ϵ ~ 6800 cm^{-1} M^{-1}) and 306 nm (ϵ = 13 000), respectively. The assignment of the IL band is based on a similar 213-nm absorption in Na(silox). A similar D_{3h} d^0 complex, (silox)$_3$TaH$_2$,[23] exhibits only two bands at 218 (ϵ = 5100 cm^{-1} M^{-1}) and 278 nm (ϵ = 4400 cm^{-1} M^{-1}), again assigned as IL and LMCT. The latter LMCT band is blue-shifted relative to **1** since the Ta(V) complex effects a stronger ligand field. EHMO calculations performed on (HO)$_3$Ta (**1′**), modeling **1**, indicate that D_{3h} symmetry is preferred over pyramidal (C_{3v}) or T-shaped (C_{2v}) structures; thus, the spectral features pertain to a D_{3h} core. Subtle deviations of the Ta-O-Si linkages from linearity are likely to manifest themselves by lifting the degeneracies of orbitals involved in π-bonding, thereby lowering the overall symmetry of the system.

The blue color of **2** originates from a transmission window near 480 nm while its pale appearance is due to the weak character (ϵ = 36 cm^{-1} M^{-1}) of the only absorption in the visible region, centered at 612 nm (16 300 cm^{-1}). Two subtle shoulders on this band are also evident at ~570 (17 500 cm^{-1}, $\epsilon \leq 5$ cm^{-1} M^{-1}) and ~695 nm (14 700 cm^{-1}, ϵ ~ 25 cm^{-1} M^{-1}). In the near-IR region, a broad absorption is centered at 928 nm (10 780 cm^{-1}, ϵ = 34 cm^{-1} M^{-1}) with an accompanying shoulder at 840 nm (11 900 cm^{-1}, ϵ ~ 25 cm^{-1} M^{-1}). These broad, weak bands are tentatively assigned as triplet absorptions arising from the $a_1'^2 \rightarrow a_1'^1e''^1$ transition. Rigorously, only one triplet ($^1A_1' \rightarrow {}^3E''$) results from this electron configuration; however, any distortion from D_{3h} symmetry will split the e″-type orbitals, resulting in two bands. The energy difference between the two bands tends to argue against splitting due to spin–orbit coupling, since λ(Ta^{III}) is estimated to be ~1400 cm^{-1},[73] but the shoulders accompanying each absorption may manifest such features.

Several bands not obscured by the IL and LMCT absorptions appear in the near-UV at region 238 (42 000 cm^{-1}, ϵ ~ 2000 cm^{-1} M^{-1}), 350 (ϵ ~ 1000 cm^{-1} M^{-1}), 364 (27 500 cm^{-1}, ϵ ~ 2400 cm^{-1} M^{-1}) and 394 nm (ϵ ~ 1100 cm^{-1} M^{-1}), each possessing similar extinction coefficients. The 238-nm band is assigned as the *xy*-allowed $^1A_1' \rightarrow {}^1E'$ ($a_1'^2 \rightarrow a_1'^1e'^1$) transition, since it appears at nearly twice the energy of the corresponding band in the related d^1 (silox)$_3$Ti (**2**) complex (20 000 cm^{-1}).[29] The covalent radii of Ti (1.32 Å) and Ta (1.34 Å) are similar, and ligand fields of second- and third-row elements are typically about twice the magnitude of analogous first-row species.[73] The 364-nm band is assigned as the electric-dipole-forbidden $^1A_1' \rightarrow {}^1E''$ ($a_1'^2 \rightarrow a_1'^1e''^1$) transition, presumably strong due to intensity stealing from the charge-transfer absorptions, vibronic coupling, and the breakdown from rigorous D_{3h} symmetry. One of the neighboring bands could also result from slight splitting of the e″ orbitals.

From the convention of Wood,[74] and the above assignments, the orbital energies may be estimated as follows: a_1' (d_{z^2}), −29 500 cm^{-1}; e″ (d_{xz}, d_{yz}), −2040 cm^{-1}; e′ (d_{xy}, $d_{x^2-y^2}$), 16 800 cm^{-1}.[75] The resulting CFSE of −59 000 cm^{-1} reveals that the silox groups

(70) (a) Saunders, J. K. N.; Hunter, B. *Modern NMR Spectroscopy*; Oxford University Press: New York, 1987. (b) Leyden, D. E.; Cox, R. H. *Analytical Applications of NMR*; Wiley-Interscience: New York, 1977.
(71) For a recent application of the technique, see: Tracey, A. T.; Li, H.; Gressner, M. J. *Inorg. Chem.* **1990**, *29*, 2267–2271.
(72) Corbin, D. R.; Willis, W. S.; Duesler, E. N.; Stucky, G. D. *J. Am. Chem. Soc.* **1980**, *102*, 5971–5973.
(73) Figgis, B. N. *Introduction to Ligand Fields*; Interscience: New York, 1966.
(74) (a) Wood, J. S. *Inorg. Chem.* **1968**, *7*, 852. See also: (b) Kŏnig, E.; Kremer, S. *Ligand Fleld Energy Diagrams*; Plenum Press: New York, 1977.
(75) For a spectral analysis of related first-row [(Me$_3$Si)$_2$N]$_3$M species, see: (a) Alyea, E. C.; Bradley, D. C.; Copperthwaite, R. G.; Sales, K. D. *J. Chem. Soc., Dalton Trans.* **1973**, 185–191. (b) Fenton, N. D.; Gerloch, M. *Ibid.* **1988**, 2201–2210.

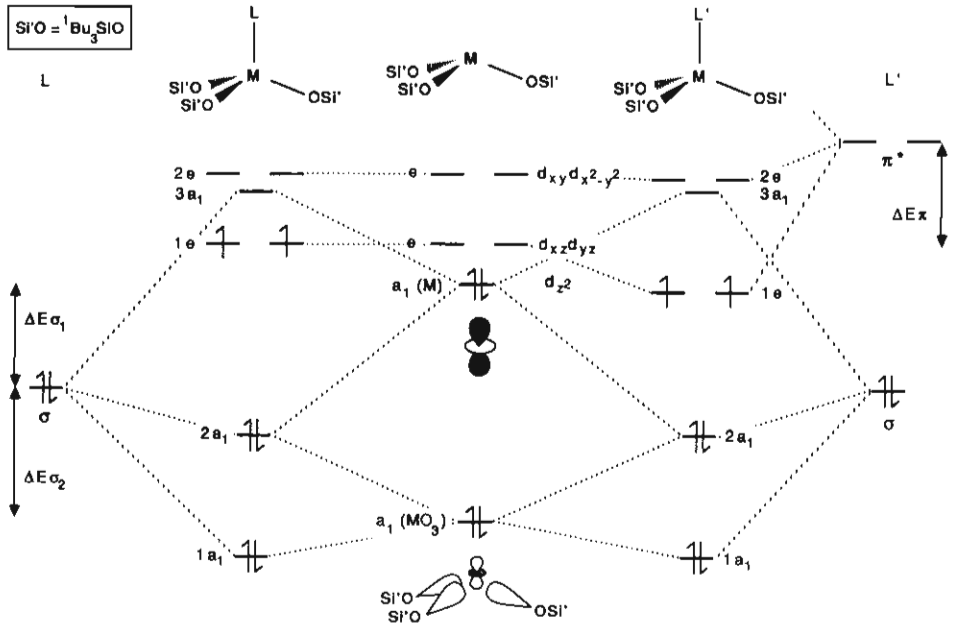

Figure 4. Simplified molecular orbital diagram for d^0–d^2 $(silox)_3M$ species and a simple σ-donor (L) or one with π-bonding capability (L').

impart a very strong ligand field about $(silox)_3Ta$ (**1**). Two other features of the d-orbital energetics warrant attention. First, the d_{z^2} orbital is extremely low in energy, indicative of minimal σ^* character, thus the d-electron density is located above and below the TaO_3 plane. Second, the relative energy of the e'' set is extremely high, supporting the contention that silox is an effective π-donor. Together, these energy levels are inverted, but comparably separated with respect to levels of a typical third-row d^8 tbp complex.

Ligation of $(silox)_3Ta$ (1). The substantial reducing power[23] and steric properties of $(silox)_3Ta$ (**1**) are clearly manifested in the unusual binding modes found for the pyridine derivatives, the ditantallobenzene complex (**7**), and the various olefin and alkyne complexes. By binding ligands in an η^2-fashion, the Ta can achieve its highest formal oxidation state. The tantalum–carbon and –nitrogen bond distances in $(silox)_3Ta(\eta^2\text{-}NC_5H_5\text{-}N,C)$ (**10a**) and $[(silox)_3Ta]_2\{\mu\text{-}\eta^2(1,2):\eta^2(4,5)\text{-}C_6H_6\}$ (**7**) are similar to σ-bonds, corroborating the metallaaziridine[55-57] and metallacyclopropane depictions.[35-37] In these cases, formation of σ-interactions (i.e., η^2-bonds) compensates for the disruption of resonance stabilization energy (py: ~28 kcal/mol;[76] ~35 kcal/mol),[77] although it is difficult to assess how much is lost upon coordination. Note that a Ta(V) resonance depiction of a hypothetical η^1-pyr complex requires the ligand to be zwitterionic (i.e., $(silox)_3Ta{=}{}^{+}\overline{N{-}CH{=}CH{-}CH^{-}{-}CH{=}CH}$). The calculations described herein reveal that the inability of an η^1-pyridine to back-bond effectively is a key feature in determining adduct geometry.

EHMO calculations on pyramidalized (C_{3v}) $(HO)_3M$ fragments[78,79] provide a general rationale for ligation of a trigonal d^n metal center. Figure 4 schematically illustrates the general situation for d^0–d^2 $(silox)_3M$ species and a simple σ-donor (L) or one with π-bonding capability (L'). For a pure σ-donor ligand, two orbital interactions are critical. The first, labeled $\Delta E(\sigma_1)$ (i.e., $E(a_1(M)) - E(\sigma)$), corresponds to the interaction of the ligand donor pair (σ) with a filled d_{z^2} orbital of the pyramidalized $(silox)_3M$ fragment ($a_1(M)$). In the figure, $3a_1$ has been arbitrarily placed slightly below 2e; depending on the strength of interaction $\Delta E(\sigma_1)$, it may be higher than 2e. In any case, the pseudotetrahedral order would prevail. The second crucial interaction, designated as $\Delta E(\sigma_2)$ (i.e., $E(\sigma) - E(a_1(MO_3))$), involves the ligand σ-orbital and an orbital comprised of the symmetric combination of silox oxygen sp hybrids with a minor contribution from the metal d_{z^2} orbital. Once combined, these orbitals generate the $1a_1$, $2a_1$, and $3a_1$ molecular orbitals of a $(silox)_3ML$ complex. For a d^2 complex, these four-electron repulsive interactions present complementary problems. Since each fragment orbital is filled, ligation by L can occur only because $3a_1$ is higher in energy than 1e, the HOMO for $(silox)_3ML$. The stabilization of σ and $a_1(MO_3)$ as $2a_1$ and $1a_1$ is somewhat offset by the population of 1e, which is at higher energy than $a_1(M)$. For $(silox)_3Ta$ (**1**), the UV–vis spectrum revealed that e'' was very high in energy; thus, the population of the corresponding 1e orbital for $(silox)_3TaL$ will be significantly destabilizing.

For M = Sc, σ and $a_1(MO_3)$ are stabilized in the aforementioned fashion, and the binding of an additional ligand L is strongly preferred over the three-coordinate alternative, since $a_1(M)$ is unoccupied. In a $(silox)_3TiL$ (**2**-L) derivative, the 1e orbital is only half-populated; hence, adduct formation is still favored, but the net stabilization is predicted to be somewhat weaker than in the Sc case. For the d^0 and d^1 cases, the interaction energetics (i.e., $\Delta E(\sigma_1)$, $\Delta E(\sigma_2)$) and orbital overlaps need not be emphasized, but for the d^2 examples, they become crucial. For example, the lower ionization energies of the Ta(III) fragment, relative to V(III), differentiate their behavior, since $\Delta E(\sigma_1)$ will be greater. For $(silox)_3Ta$ (**1**), severe four-electron repulsion problems exist; because $\Delta E(\sigma_1)$ is large, the stabilization of σ as $2a_1$ is minimal, in part due to mixing with the filled $a_1(TaO_3)$ orbital. The half-occupation of 1e and the entropic problems of binding L render **1** three-coordinate. In contrast, $a_1(V)$ of $(silox)_3V$ (**4**) interacts strongly with σ because of the smaller $\Delta E(\sigma_1)$, leading to greater stabilization of $1a_1$ and $2a_1$, enough to overcome half-population of 1e and the entropy of binding. Furthermore, if L is a π-donor (not illustrated), the filled 1e HOMO constitutes a major π^* component of the $O(p\pi) \rightarrow M(d\pi)$ bonding; since π-overlaps tend to be much more significant for third-row vs first-row transition metals, occupation of these orbitals has a stronger antibonding contribution in the tantalum case. This effect is manifested by $(silox)_3Ta$ (**1**), whose $^1A_1'$ ground state (D_{3h}) is possible because π-bonding has rendered e'' much higher than a_1' in energy. In contrast, hypothetical $(silox)_3V$ (**4**) would be expected to have e'' nearer a_1' in energy, because of relatively diminished π-effects.

While σ-adducts of $(silox)_3Ta$ (**1**) are apparently not stable, π-accepting ligands, such as olefins and alkynes, bind tightly to

(76) Gilchrist, T. C. *Heterocyclic Chemistry*; Pitman: London, 1985; p 19.
(77) (a) Benson, S. W. *Thermochemical Kinetics*; John Wiley and Sons: New York, 1968. (b) George, P. *Chem. Rev.* **1975**, *75*, 85–112.
(78) Dedieu, A.; Albright, T. A.; Hoffmann, R. *J. Am. Chem. Soc.* **1979**, *101*, 3141–3151.
(79) Albright, T. A.; Burdett, J. K.; Whangbo, M.-H. *Orbital Interactions in Chemistry*; John Wiley: New York, 1985.

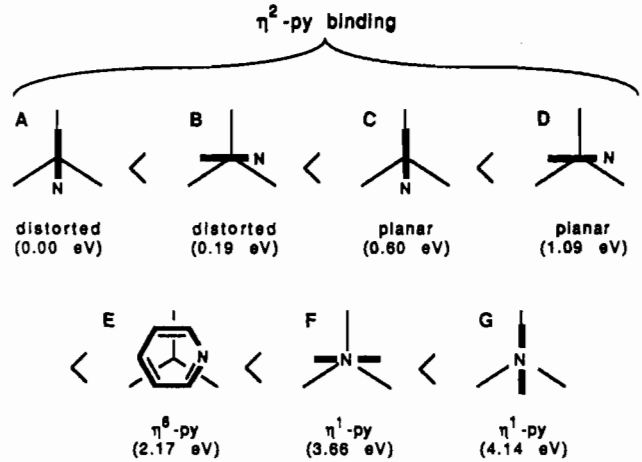

Figure 5. Seven possible binding modes of pyridine (distorted, C(2) pyramidalized, H(2) pointed out of the py plane; planar, H(2) in py plane). In A–D, the bold line indicates the η^2-N,C bond; the remainder of the η^2-py is not shown. In A–D, the py plane is taken to form an angle of 135° with the Ta–N–C(2) plane.

the tantalum center. Consider a cylindrically symmetric L′ that possesses two π^* orbitals (e.g., CO),[23] as Figure 4 indicates. Interaction of these orbitals with the lower e-set (d_{xz}, d_{yz}) of the pyramidal (silox)$_3$M fragment results in a significantly stabilized 1e HOMO. If this additional stabilization is enough to overcome the four-electron repulsion problems pertaining to σ-bonding and the unfavorable entropy of binding, formation of the adduct is favored. Olefins break the 3-fold symmetry of the molecule and split the degeneracy of the 1e set, leading to one filled, greatly stabilized orbital. The metallacyclopropane depiction common to early-transition-metal–olefin complexes represents the extreme of this back-bonding interaction.[35-37] Alkynes behave similarly, except for the added complexity of CC($\pi_\perp$) → Ta(dδ) δ-bonding.[48-51]

EHMO calculations on the hypothetical [(HO)$_3$Ta]$_2${μ-η^2-(1,2):η^2(4,5)-C_6H_6} (**7′**) analogue of **7** revealed that the bis-η^2 arrangement was marginally more stable than the corresponding bis-η^1 or -η^3 geometries.[41,42] However, a μ-η^6:η^6 sandwich complex analogous to [CpV]$_2$(μ-η^6:η^6-C_6H_6)[4] was predicted to be a more favorable energetically by a substantial amount. Unfavorable steric interactions between the silox ligands of facially oriented η^6-coordinated (silox)$_3$Ta groups presumably prevent this possibility. Calculations on **7′** also indicated a diamagnetic ground state in which a large amount of electron density resides on the unbound carbons in the HOMO. Recent Fenske–Hall MO calculations by Wigley et al.[17] on a related complex, (PhO)-Cl_2Ta(η^6-C_6H_6), indicated the expected distortion toward a metallanorbornadiene structure (i.e., 1,4-dienediyl) that manifests strong Ta(dδ) → C_6H_6(π^*) back-bonding and rather weak C_6H_6(π) → Ta(dπ) bonding. It is plausible that the related (silox)$_3$Ta(η^6-C_6H_6) complex is not observed because of steric constraints.

Electronic Structure of (silox)$_3$Ta(η^2-NC_5H_5-*N,C*) (10a). In order to gain more insight into the unprecedented orientation of the pyridine ligand, EHMO calculations were performed on the hypothetical (HO)$_3$Ta(η^2-NC_5H_5-*N,C*) (**10a′**) analogue of **10a**. The (HO)$_3$Ta geometry was taken from the crystal structure of **10a**, and distances from gaseous pyridine were used.[54] Shown in Figure 5 are seven possible binding modes for pyridine, ordered from left to right by increasing energy. Orientations A–D represent η^2-bound rotomers with either distorted (i.e., C(2) pyramidalized, H(2) pointed out of the py plane) or planar (i.e., H(2) in py plane) pyridine geometries, whereas F and G denote η^1-binding and E illustrates a representative η^6-interaction. The η^2-geometry is universally preferred over the alternative structures, and the most stable configuration (A), where the η^2-N,C unit is aligned with a Ta–O bond and N trans to a silox, is closest to the observed solid-state structure (Figure 2). In addition to the seven models, the py ring in A and C was rotated 180° to reverse the N and C(2) positions. The MO diagrams of these species appeared similar to A and C and thus were not treated individually, although the new distorted and planar structures were found to be 0.20 and 0.43 eV greater than their counterparts, respectively, principally due to the asymmetry of the pyramidal (HO)$_3$Ta fragment molecular orbitals. Since these deviations are not germane to the η^2- vs η^1-bonding question, they were not addressed. The relative energies of A–D increase as the energies of their respective HOMO's rise and as the HOMO–LUMO gaps decrease. These trends hint at the importance of these orbitals, particularly the HOMO, in determining the electronic factors that are critical to the geometry of **10a**.

Figure 6 illustrates two interaction diagrams for (HO)$_3$Ta-(η^2-NC_5H_5-*N,C*) (**10a′**) in which the η^2-N,C bond is aligned with a TaO linkage. The diagrams have been truncated to include only the d block of pyramidal (HO)$_3$Ta[78,79] and those pyridine σ and π orbitals critical to the complexation. On the left side of the figure, the py ligand that interacts with pyramidal (HO)$_3$Ta has been distorted at C(2) (i.e., A); hence, the labels contain the superscript d, whereas the py on the right has remained planar (i.e., C). Other than slight shifts in energy, the ligand orbitals undergo two critical changes upon bending H(2) out of the pyridine plane. Due to substantial mixing with numerous σ-orbitals, the N^d HOMO develops approximate radial p character at C(2) not observed in the undistorted HOMO N, and becomes directionalized for η^2-ligation. Its energy rises nearly 0.5 eV, thereby reducing the difference between it and the Ta d orbitals. The second change comes in the π_4^d LUMO, which gains C(2) character from mixing with π_5 and is slightly stabilized. Although the distortion raises the total pyridine energy by 1.26 eV, compensation via η^2-complexation is considerable.

The hypothesis that the relative stabilities of A and C are determined by their HOMO's is borne out in a comparison of their molecular orbital diagrams. Except for the HOMO's, the occupied orbitals are at comparable energies. This is fortuitously true even for the two ψ_1's that are derived from pyridine HOMO's N^d and N. Although the additional C(2) character of N^d accounts for a stronger interaction with the tantalum, this is counteracted by the initial destabilization due to the distortion at C(2). The composition of the two orbitals reflects the vast difference in the extent of metal–ligand interaction; ψ_1(A) and ψ_1(C) are comprised of 23% and 4% (HO)$_3$Ta character, respectively.

The HOMO's of A and C, labeled ψ_2, both result primarily from a bonding interaction between π_4^d (π_4) and one of the 1e tantalum-based orbitals. The HOMO of (HO)$_3$Ta (2a), mostly d_{z^2} in character, is pushed up strongly through mixing with numerous occupied pyridine orbitals. Several factors contribute to a greater stabilization of ψ_2(A) versus ψ_2(C). The distorted pyridine orbital π_4^d is lower in energy than π_4, thereby providing a better energy match with the (HO)$_3$Ta 1e set, and possesses a larger C(2) coefficient for greater overlap. In addition to π_4^d (π_4) and 1e, the HOMO's of A and C contain significant contributions from N^d and the 2e set, respectively. The former interaction is destabilizing, but a large contribution from π_4^d (40%) to ψ_2(A) counteracts that of the N^d, resulting in a net stabilization. In contrast, ψ_2(C) incurs a net destabilization because the contribution of π_4 (28%) is not enough to overcome an energy increase due to mixing with other occupied pyridine orbitals. The enhanced interaction of 1e with π_4^d provides the major energetic impetus for the out-of-plane H(2) distortion contracted via η^2-pyridine ligation.

The stronger π_4^d mixing in A is manifested in the TaN and TaC(2) bond strengths, as indicated by the overlap populations (op) of ψ_1 and ψ_2. In A, ψ_1 and ψ_2 have overlap populations of 0.044 and 0.036 toward a total op of 0.534 for the TaN bond, whereas ψ_1 and ψ_2 contribute 0.016 and 0.009 toward the 0.526 total in C. For the TaC(2) bond, ψ_1 and ψ_2 provide 0.071 and 0.146, the latter due to the enlarged C(2) component of π_4^d, toward the 0.487 total in A, yet only 0.021 and 0.020 toward the 0.352 total overlap population in C. Clearly, pyramidalization at C(2) is a major contributor toward η^2-coordination. An important agostic interaction[58] was expected for the planar coordinated

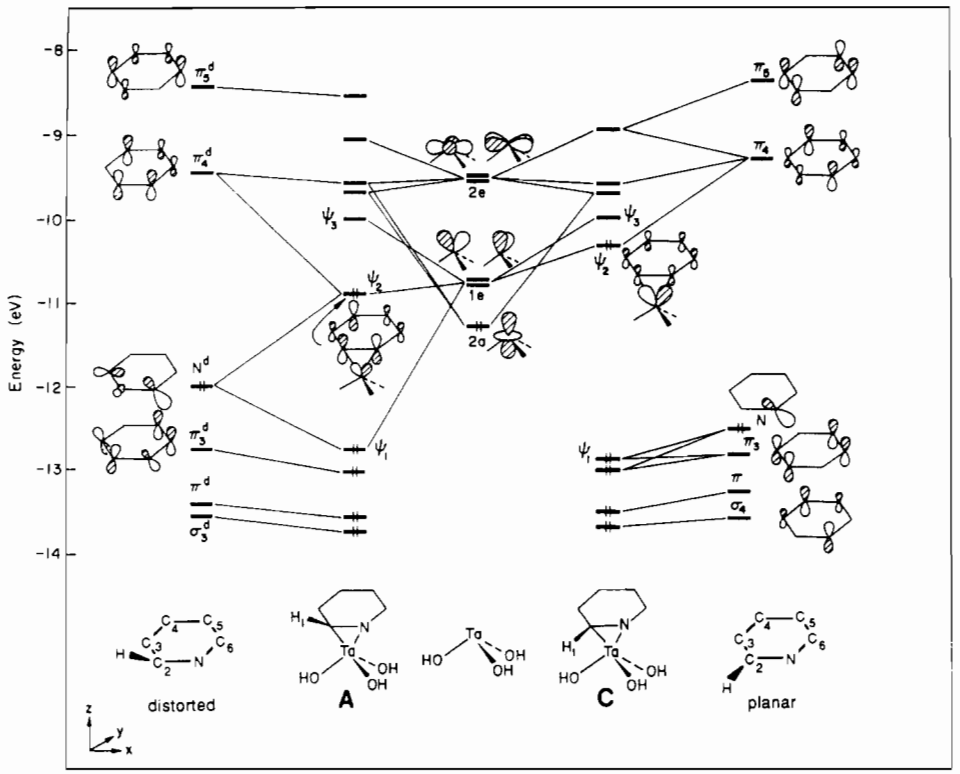

Figure 6. Truncated molecular orbital diagram for the hypothetical $(HO)_3Ta(\eta^2\text{-}NC_5H_5\text{-}N,C)$ (**10a'**), a model for $(silox)_3Ta(\eta^2\text{-}NC_5H_5\text{-}N,C)$ (**10a**), indicating the distorted (A) and planar (C) η^2-bonding modes of pyridine.

pyridine structure (C), since the TaH(2) distance was estimated to be 1.86 Å. However, while the TaH op is large (0.16), this character is spread over a number of MO's and their stabilization is insufficient to outweigh the considerable differences in HOMO energies.

Since bond distances of free pyridine were used in the calculations,[54] changes in the overlap populations of the C–C and C–N bonds upon complexation inversely mirror the changes in bond lengths observed in the crystal structure of $(silox)_3Ta(\eta^2\text{-}NC_5H_5\text{-}N,C)$ (**10a**). For example, the C(2)–N bond length of 1.43 Å is 0.09 Å greater than the corresponding free pyridine distance, while the op pertaining to C(2)–N decreases (–0.19) upon ligation. The remaining η^2-pyridine distances (Figure 2) experience a similar correlation: C(2)–C(3), 0.14 Å, Δ(op) = –0.18; C(3)–C(4), –0.08 Å, Δ(op) = 0.10; C(4)–C(5), 0.04 Å, Δ(op) –0.01; C(5)–C(6), –0.06 Å, Δ(op) 0.07; C(6)–N, 0.10 Å, Δ(op) –0.07. These correlations arise from the population or depopulation of the distorted pyridine fragment molecular orbitals (FMO's) upon complexation and are not present in a comparison of the distorted and planar pyridines.

The two remaining η^2-compounds, B (distorted py) and D (planar py), in which the N-C(2) linkage is perpendicular to a Ta–O vector, are described by a set of molecular orbital diagrams nearly identical with those in Figure 6. It does not appear possible to rationalize the preference between the aligned and perpendicular geometries on the basis of the electronic structure alone; thus, steric forces may play a more forceful role. It is interesting to note that the bond distortions derived from the op changes in the pyridine fragments of B and D do not agree with the observed structure as closely as A and C. Inspection of the pyridine fragment MO occupations and the characters and energies of the MO's revealed that this anomaly can be explained, but the details are subtle and this discussion is addressed elsewhere.[44]

The greater stability of the η^2-distorted pyridine complex (A) over its planar counterpart (C) originates from three major factors: (1) the exaggerated C(2) lobes of both N^d and $\pi_4{}^d$ that lead to improved overlap; (2) the superior energy match of both N^d and $\pi_4{}^d$ to the appropriate $(HO)_3Ta$ orbitals; (3) the energetically ineffective agostic interaction in the η^2-planar case. These features essentially describe a metallaaziridine,[55-57] the structure in which

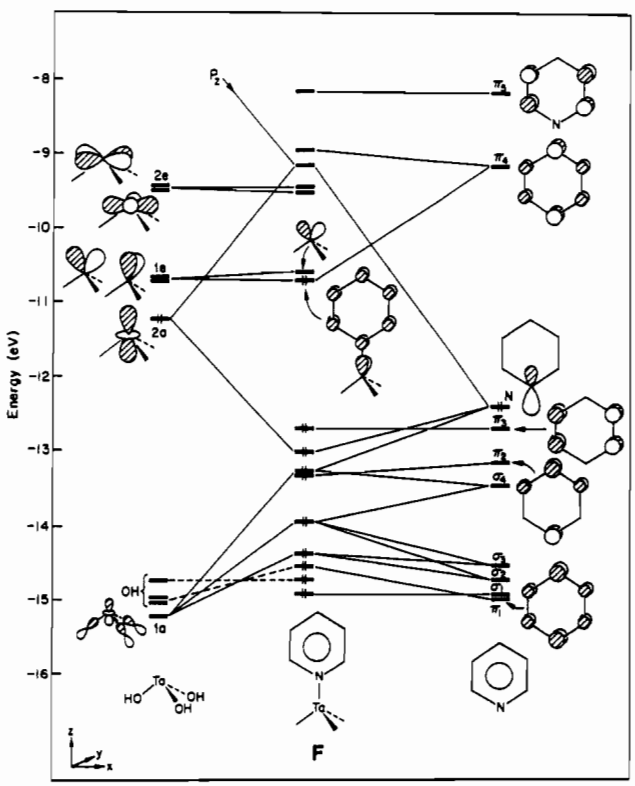

Figure 7. Truncated molecular orbital diagram for the hypothetical $(HO)_3Ta(\eta^1\text{-}NC_5H_5)$ (F).

π-back-bonding to pyridine has been maximized.

Electronic Structures of Hypothetical $(HO)_3Ta(\eta^1\text{-}NC_5H_5)$ (F, G) and $(HO)_3Ta(\eta^6\text{-}NC_5H_5)$ (E). Illustrated in Figure 7 is the molecular orbital diagram of $(HO)_3Ta(\eta^1\text{-}NC_5H_5)$ (F), in which the CNC unit is perpendicular to a TaO bond. The electronic situation for G is so similar to that for F that only one need be addressed. One striking feature of the diagram concerns the small

Table IV. Comparison of the Composition of HOMO's for $(HO)_3Ta(py)$ (A–G) in Percent

binding mode	structure	% composition: pyridine FMO's π_5^d	π_4^d	N^d	tot. pyridine	tot. $(HO)_3Ta$
η^2	A	0	40	20	68	32
	B	4	45	23	77	23
	C	5	28	1	42	58
	D	10	23	2	45	55
η^6	E	0	36	0	38	62
η^1	F	0	6	0	10	90
	G	0	6	0	10	90

HOMO–LUMO gap (0.043 eV). In contrast to the η^2-cases, the $(HO)_3Ta$ 1e set is ineffectively split by interaction with the π_4 orbital of pyridine, which contributes only ~6% of the orbital density in the HOMO. Furthermore, because of the higher symmetry of F, π_5 cannot mix with and help stabilize the metal-based orbitals as it does for the η^2-geometries. In essence, the diagram reveals the poor π-accepting capability of pyridine.

Although the ground state of F is depicted as a singlet, the 1e splitting may be small enough to produce a triplet. Recall that the vanadium derivative, (silox)$_3$Vpy (**4**-py) possesses a triplet ground state; in this case, the splitting should be virtually nonexistent, since the π_4/1e energy match is far worse and the π-overlap for py and a first-row metal should be poor. Since titanium is more electropositive than vanadium, but less than tantalum, (silox)$_3$Ti(py) (**2**-py) represents an intermediate case. The π-back-bonding involving π_4 is insufficient to generate an η^2-geometry because of only moderate overlap, energetics that are unfavorable relative to **10a**, and the population of the HOMO by only one electron. η^1-Pyridine binding to titanium is predictable and consistent with moderate electron density on py, since the HOMO will have a minor pyridine component.

The major component to η^1-binding is the σ-donation by the nitrogen lone pair, the orbital generated upon mixing the 2a d_{z^2} and N. Relative to N, the molecular orbital is stabilized ~0.5 eV and slips below the nonbonding π_3 MO. A series of four-electron, two-orbital destabilizing interactions originates with the d_{z^2} character of the HO bonding orbitals, 1a. Although mainly localized on the oxygen p orbitals, this FMO has sufficient d_{z^2} character to couple strongly with σ_1–σ_4, which incur strong destabilization in contrast with the η^2-cases, where they remained essentially nonbonding. In addition, if the Ta–N distance, which was arbitrarily set to be equivalent to the η^2-Ta–N distance, is shortened, 1a will begin to repel the nitrogen lone pair orbital as previously discussed (Figure 4).

In summary, F and G are unfavorable structures for two major reasons: (1) the ineffective stabilization of 1e by π_4 that leads to a small HOMO–LUMO gap; (2) the strong four-electron, two-orbital destabilization of the pyridine σ-orbitals.

The molecular orbital diagram of the η^6-coordinated pyridine will not be detailed,[44] in part because arene coordination has already been addressed by Wigley et al.[17] and the interpretations are very similar. In the η^6-bonding mode, there is a complete lack of N and σ-orbital stabilization, two obvious factors that weigh against its observation. Compensation by strong donation from the occupied π orbitals of the ring usually occurs, but for $(HO)_3Ta$, the strong overlaps necessary for π-type coordination are energetically unfavorable in contrast to later transition metals, where η^6-arene complexes are relatively common. The π-accepting orbitals of the pyridine fragment, π_4 and π_5 (refer to Figure 7), overlap inadequately with 1e, but satisfactory with 2e; thus, the HOMO of the system has Ta(dδ) → py(π^*) back-bonding character. The latter, in combination with minor π-donation of π_2 and π_3 to the 1e orbital, is enough to favor η^6-bonding over η^1, but remains far short of competing with η^2-pyridine bonding.

Comparison of η^2-, η^6-, and η^1-Pyridine Structures. Several points about structures A–G are best made by direct comparison, especially those pertaining to the character of the HOMO's. Table IV manifests the composition of the seven HOMO's in terms of the contributions from the pyridine FMO's as well as from the entire $(HO)_3Ta$ and pyridine units. From inspection of the table, it is clear that the HOMO's of the η^2-structures are more evenly divided between the pyridine and $(HO)_3Ta$ fragments, a testament to greater bonding. In contrast, the η^1-HOMO's are best described as nonbonding, metal-based orbitals. Differences in the distorted and planar pyridine structures are also apparent, because the former carry a much larger N^d component as well as a greater total contribution from the pyridine. Examination of the FMO occupations across the series corroborates these findings, indicating the π-accepting ability of the pyridine ligand varies as $\eta^2 > \eta^6 > \eta^1$. As expected, the N-donation varies as $\eta^1 > \eta^2 > \eta^6$, and the π-donation by the ring orbitals follows the trend $\eta^6 > \eta^2 > \eta^1$. The lack of involvement by the π orbitals, both π^b and π^*, in the η^1-structure certainly hampers its observation.

η^2-Coordination vs 4-CH Activation of Pyridine. Recall that the pyridyl–hydride (silox)$_3$Ta(H)($C_5H_2Me_2N$) (**11a**) was the first product formed upon exposure of (silox)$_3$Ta (**1**) to 2,6-lutidine (eq 10); rearrangement to the η^2-2,6-lutidine structure, (silox)$_3$Ta(η^2-2,6-$NC_5H_3Me_2$-*N*,*C*) (**11b**; eq 11), occurred subsequently. Figures 6 and 7 reveal that the pyridine π_4 and $(HO)_3Ta$ 2a orbitals are only ~2 eV apart. Furthermore, the coefficient on C(4) is greater than the coefficients of C(2,6) and C(3,5), and somewhat greater than the coefficient on N, since the orbital reflects the inductive effect of the more electronegative nitrogen. Scheme II indicates that nucleophilic attack by the pair of electrons in 2a toward the C(4) position on the lutidine (I)[80] presents a plausible scenario for the initial step of CH activation. Harman and Taube have investigated related substituent effects on the η^2-C,C′-binding of arene ligands.[11] The ensuing transfer of hydride to tantalum completes the mechanism for the generation of **11a**, one that is reminiscent of Graham's proposed arenium intermediate to arene CH activation.[8]

The observation of the pyridyl–hydride complex and the corresponding molecular orbital rationale pose some interesting questions. While it is reasonable to assume that steric inhibition of η^2-$NC_5H_3Me_2$-*N*,*C* binding enables the observation of CH activation (vide supra), this pathway should be feasible for all pyridine substrates that are not blocked in the 3-, 4-, and 5-positions. It is likely that the slow rate of 4-CH activation and the thermodynamic instability of the aryl–hydrides relative to unhindered η^2-N,C adducts (e.g., **10a** and **10b**) renders such products unobservable in most cases. The 2,6-lutidine C–H activation also suggests that η^2-$NC_5H_3R_2$-*N*,*C* (R = alkyl, H) structures may be similarly formed. Nucleophilic attack by the 2a electrons of $(HO)_3Ta$ at C(2) or C(6), which both have substantial coefficients in π_5 (Scheme II, II), would lead to a zwitterionic species that collapses to the η^2-geometry. This zwitterionic species represents the extreme view of an asymmetric attack at the N=C unit[81] and thus may not be a true intermediate. Regardless, the four-electron repulsion problems that occur when the midpoint of the NC bond or the N lone pair directly approaches the tantalum center may be obviated via an asymmetric approach.

In view of the LUMO-directed asymmetric attack of the N=C unit pyridine delineated above, EHMO calculations of pyridazine (1,2-$N_2C_4H_4$) and pyrimidine (1,3-$N_2C_4H_4$) were conducted. Attack by electrons in the d_{z^2} orbital of (silox)$_3$Ta (**1**) at the LUMO's of these heterocycles is predicted to yield the observed products, (silox)$_3$Ta(η^2-$N_2C_4H_4$-*N*,*N*′) (**12**; eq 12), and (silox)$_3$Ta(η^2-1,3-$N_2C_4H_4$-*N*^{1},*C*^{6}) (**13**; eq 13), thereby corroborating the frontier orbital interpretation.

Summary

The experiments and calculations clearly point to the importance of four-electron repulsions in determining the three coordinate character of (silox)$_3$Ta (**1**), whose siloxide ligands affect a strong ligand field. Only ligands with π-accepting orbitals are predicted to bind to the d^2 metal center, and those may be subject to

(80) Abramovitch, R. A. Pyridine and Its Derivatives. In *Heterocyclic Compounds*; Newkome, G. R., Strekowski, L., Eds.; Wiley & Sons: New York, 1975; Vol. 14.
(81) Eisenstein, O.; Hoffmann, R. *J. Am. Chem. Soc.* **1981**, *103*, 4308–4320.

Scheme II

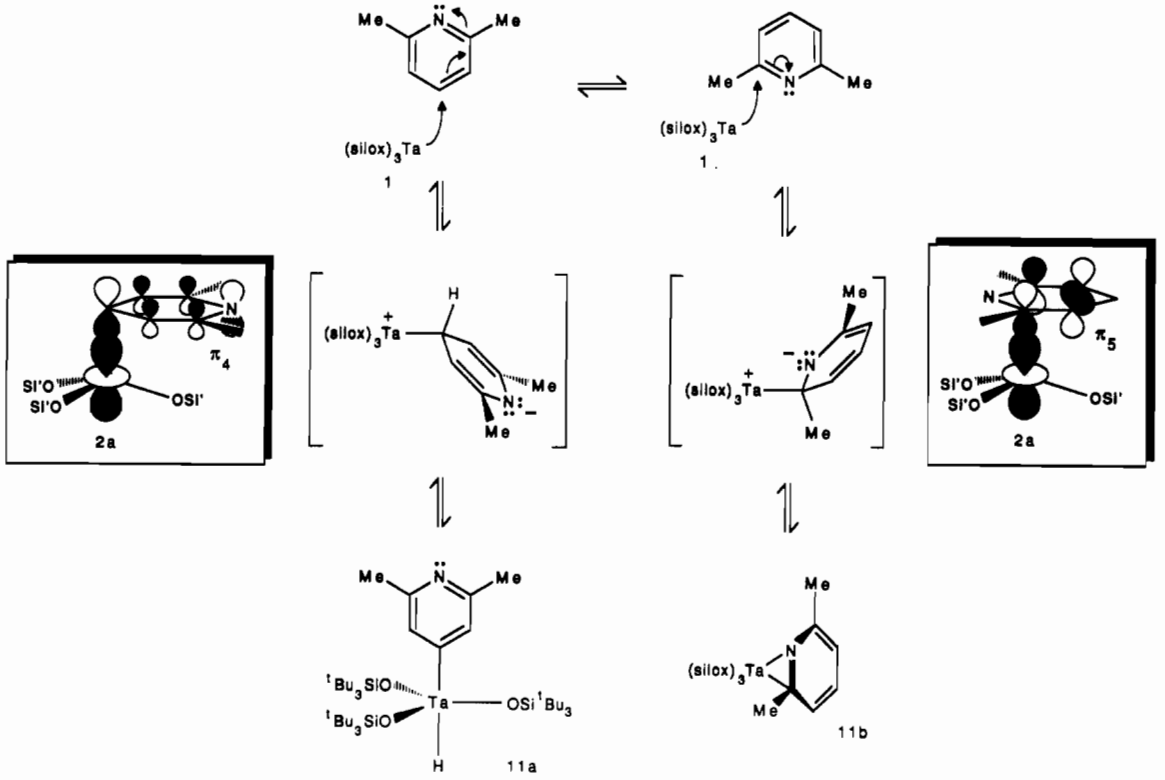

two-electron reduction, as evidenced by the binding of pyridine as a metallaaziridine. Less electropositive metals such as V and Ti react in a more conventional manner because they do not exhibit substantial electron–electron repulsion problems upon coordinating a fourth ligand to the $(silox)_3M$ fragment and manifest weaker π-interactions. The highly electropositive $(silox)_3Sc$ (**3**) fragment does not suffer the same fate as **1**, because critical four-electron repulsion problems disappear when the metal center is d^0.

Experimental Section

General Considerations. All manipulations were performed by using either glovebox or high-vacuum-line techniques. Ethereal and hydrocarbon solvents were distilled under nitrogen from purple sodium benzophenone ketyl and vacuum transferred from the same prior to use. Benzene-d_6 and pyridine-d_5 were dried over activated 4-Å molecular sieves, vacuum transferred, and stored under N_2; THF-d_8 was dried over sodium benzophenone ketyl. Argon and hydrogen were passed over MnO on vermiculite and activated 4-Å sieves. Acetylene was separated from the acetone stabilizer by passing it through two −78 °C spiral traps. *cis*- and *trans*-butene were purified by in vacuo condensation at 77 K followed by drying over activated 4-Å molecular sieves. Pyridine and substituted pyridines were refluxed over KOH, distilled, and then vacuum transferred from activated 4-Å molecular sieves; pyridazine and pyrimidine were purified by vacuum transfer from activated 4-Å molecular sieves. Pyridine-α-d[59] and pyrimidine-2-d[65] were prepared from literature procedures and dried as described above. NH_3 was dried over Na, and $HNMe_2$ was purchased from Matheson and used as received. Preparations of $Sc[N(SiMe_3)_2]_3$,[31] $(silox)_3Ta$ (**1**),[23] and $(silox)_3Ti$ (**2**)[29] have been described previously.

NMR spectra were obtained by using Varian XL-200 (^1H) and XL-400 (^1H (VT), $^{13}C\{^1H\}$, HETCOR) and Bruker WM-300 (^2H, $^{13}C\{^1H\}$) spectrometers. Chemical shifts are reported relative to benzene-d_6 (^1H, δ 7.15; $^{13}C\{^1H\}$, δ 128.00) or THF-d_8 (^1H, δ 1.73 and 3.58; $^{13}C\{^1H\}$, δ 67.4 and 25.3). Spin density probabilities were calculated from ^1H spectra obtained on the XL-200 instrument. Infrared spectra were recorded on a Mattson FT-IR interfaced to a AT&T PC7300 computer. UV–visible spectra were recorded on an HP 8531 diode-array spectrophotometer. Room-temperature magnetic susceptibility measurements were performed by using the Evans method.[33] Molecular weights were obtained or a home-built device for benzene cryoscopy.[82] Analyses were performed by Analytische Laboratorien, Elbach, West Germany, and Oneida Research Services, Whitesboro, NY.

(82) Wanat, R. A., Ph.D. Thesis, Cornell University, 1986.

Procedures. 1. $(silox)_3Ti(py)$ (2-py). To a flask containing 0.75 g of $(silox)_3Ti$ (**2**; 1.08 mmol) and 20 mL of hexanes was added an excess of pyridine (2 mL, 24 mmol) at −78 °C. The bright orange solution quickly turned ink blue upon warming to 25 °C. Removal of the volatiles, followed by addition of fresh hexanes, filtration, reduction of solvent, and cooling to −78 °C resulted in a dark blue powder (530 mg, 63%). IR (Nujol, cm^{-1}): 1153 (w), 1045 (w), 1018 (w), 1005 (w), 965 (m), 863 (s), 820 (s), 697 (m), 627 (s), 588 (w), 530 (w). UV–vis [hexane; λ, nm (ϵ, M^{-1} cm^{-1})] 210 (10000), 250 (7700), 440 (360), 638 (1060), 820 (920). EPR (77 K, 2-methylpentane glass): $g_{\parallel} = 1.989$, $g_{\perp} = 1.914$, $g_{iso} = 1.939$ (no Ti or N hyperfine observed). μ_{eff} (Evans' method) = 1.8 μ_B. M_r: found, 800 (calcd, 773). Anal. Calcd for $C_{41}H_{86}O_3NSi_3Ti$: C, 63.68; H, 11.21; N, 1.81. Found: C, 63.54; H, 11.31; N, 1.64.

2. $(silox)_3Sc(THF)$ (3-THF). To a flask containing 2.50 g of $ScCl_3(THF)_3$ (6.65 mmol) and 4.76 g of Na(silox) (20.0 mmol) was added 60 mL of THF at −78 °C. The solution was warmed to 25 °C and stirred for 10 h. The THF was removed under vacuum and replaced with 40 mL of hexanes. Filtration, concentration, and crystallization from hexanes at −78 °C yielded colorless **3-THF** (3.65 g, 72%). ^1H NMR (C_6D_6): V, 1.21 (CH_2, m, 4 H), 1.30 (^tBu, s, 81 H), 4.05 (OCH_2, m, 4 H); $^{13}C\{^1H\}$ (C_6D_6): δ 23.21 (SiC), 29.72 (CH_2), 30.96 (CCH_3), 75.60 (OCH_2). MS (FABS, He, Nujol matrix, m/z): 705.3 (M − C_4H_8), 633.4 (M − C_4H_8, C_4H_8O). Anal. Calcd for $C_{40}H_{89}O_3Si_3Sc$: C, 62.94; H, 11.75. Found: C, 63.28; H, 11.90.

3. $(silox)_3Sc(NH_3)$ (3-NH$_3$). To a hexane solution (~35 mL) of 1.05 g of (silox)H (4.86 mmol) was added 0.85 g of $Sc[N(SiMe_3)_2]_3$ (1.62 mmol). The solution was stirred at 25 °C under a flow of argon for 10 h. The hexane and $HN(SiMe_3)_2$ were removed by vacuum distillation. After filtration in fresh hexanes, residual (silox)H and (silox)TMS were removed by sublimation at 40 °C (10^{-4} Torr). Recrystallization form a small amount of hexanes at −78 °C yielded 0.75 g (65%) of colorless crystals. ^1H NMR (C_6D_6): δ 1.24 (^tBu, s), NH_3 not observed. $^{13}C\{^1H\}$ NMR: δ 23.21 (SiC), 30.92 (CCH_3). IR (Nujol, cm^{-1}): 3371 (w, br, NH), 3281 (w). M_r: found, 703 (calcd, 709). MS (FABS, He, Nujol matrix, m/z): 650.6 (M − C_4H_8)$^+$, 635.5 (M − C_4H_8, NH_3)$^+$. Anal. Calcd for $C_{36}H_{84}O_3NSi_{34}Sc$: C, 61.05; H, 11.95; N, 1.98. Found: C, 60.86, 61.05; H, 11.61, 11.58; N, 1.43, 1.77.

4. $(silox)_3Sc(py)$ (3-py). To a flask containing 0.51 g of $(silox)_3Sc$(THF) (0.67 mmol) and 20 mL of hexanes was added an excess of pyridine (3 mL, 37 mmol) at −78 °C. The clear, colorless solution was stirred for 2 h at 25 °C, and the volatiles were removed under vacuum. The white crystalline solid was then filtered and recrystallized from hexanes at −78 °C to provide 0.41 g (79%) of colorless crystals. ^1H NMR (C_6D_6): δ 1.26 (^tBu, s, 81 H), 6.5 (3,5-CH, m, 2 H), 6.7 (4-CH, m, 1 H), 9.0 (2,6-CH, m, 2 H). $^{13}C\{^1H\}$ NMR (C_6D_6): δ 23.33 (SiC),

30.98 (CCH_3), 124.88, 140.63, 149.13 (pyridine). IR (Nujol, cm^{-1}) 1609 (m), 1221 (w), 1194 (w), 1155 (w), 1068 (w), 1044 (w), 995 (m), 908 (s), 819 (s), 698 (m), 640 (m), 621 (s), 593 (w), 530 (w). UV–vis [hexane; λ, nm (ε, M^{-1} cm^{-1})]: 205 (5000), 255 (7000). Anal. Calcd for $C_{41}H_{86}O_3NSi_3Sc$: C, 63.95; H, 11.25; N, 1.82. Found: C, 63.75; H, 10.81; N, 1.76.

5. (silox)$_3$V(THF) (4-THF). To a 50-mL flask containing 440 mg (2.80 mmol) of VCl_3 and 2.015 g of Na(silox) (8.45 mmol, 3.02 equiv), was distilled 40 mL of THF at −78 °C. Upon warming to 25 °C, the mixture was stirred for 17 h and refluxed for an additional 12 h, changing from indigo to aqua blue. The solvent was removed and the residue dissolved in 20 mL of hexanes and filtered to give an aqua solution, and a gelatinous white solid that was repeatedly washed with 30-mL portions of hexanes until no soluble material remained. The filtrate was reduced to 5 mL and cooled to −78 °C, resulting in 1.31 g of blue crystals that were collected by filtration. Recrystallization from hot toluene afforded 1.10 g (51%) of rectangular crystals. ^1H NMR (C_6D_6): δ ~1.6 (silox, $\nu_{1/2}$ = 250 Hz), ~4.0 (THF, shoulder). $^{13}C\{^1H\}$ NMR resonances were not observed. Anal. Calcd for $C_{40}H_{89}O_4Si_3V$: C, 62.45; H, 11.66. Found: C, 63.82; H, 11.56.

6. (silox)$_3$V(py) (4-py). To a flask containing 0.80 g of 4-THF (1.04 mmol) and 30 mL of hexanes was added an excess of pyridine at −78 °C. The light blue solution quickly turned green upon warming to 25 °C. The volatiles were removed, and the resulting solid was dissolved in 25 mL of hexanes, which were then removed. The latter procedure was repeated two times to remove all traces of excess pyridine. The resulting green solid was dissolved in hexanes and filtered. The solution was concentrated, cooled to −78 °C, and filtered and the green crystals (520 mg, 65%) washed once with 3 mL of cold hexanes. ^1H NMR (C_6D_6): δ 1.8 (^{t}Bu, br s, $\nu_{1/2}$ = 350 Hz), py resonances not observed. IR (Nujol, cm^{-1}): 1606 (m), 1200 (w), 1160 (w), 1073 (w), 1050 (w), 1000 (m), 900 (s), 815 (s), 692 (m), 618 (s), 532 (w). UV–vis [hexane; λ, nm (ε, M^{-1} cm^{-1})]: 210 (11 000), 250 (9000), 450 (1500), 650 (550). Anal. Calcd for $C_{41}H_{86}O_3NSi_3V$: C, 63.43; H, 11.17; N, 1.80. Found: C, 62.11, 61.81; H, 9.80, 9.76; N, 1.94, 1.22.

7. (silox)$_3$Ta(η-C$_2$H$_4$) (5a). A flask containing 355 mg of (silox)$_3$Ta (1; 0.429 mmol) dissolved in 15 mL of hexanes at 25 °C was exposed to an excess of ethylene (200 Torr, ~10 mmol). The pale blue solution rapidly turned yellow. After the solution was stirred for 5 min, the volatiles were removed until ~3 mL remained. The solution was filtered, cooled to −78 °C, and filtered to yield 230 mg yellow-orange microcrystals (63%). ^1H NMR (C_6D_6): δ 1.23 (^{t}Bu, s, 81 H), 2.32 (C_2H_4, s, 4 H). $^{13}C\{^1H\}$ NMR: δ 23.32 (SiC), 30.68 (CCH_3), 66.18 (C_2H_4, J_{CH} = 143 Hz). Anal. Calcd for $C_{38}H_{85}O_3Si_3Ta$: C, 53.36; H, 10.02. Found: C, 53.15; H, 9.88. M_r: found 850 (calcd 854).

8. (silox)$_3$Ta(η-C$_2$H$_3$Me) (5b). A flask containing 350 mg of (silox)$_3$Ta (1, 0.423 mmol) dissolved in 15 mL of hexanes at 25 °C was exposed to an excess of propylene (400 Torr, ~20 mmol). The pale blue solution rapidly turned orange. After the solution was stirred for 35 min, the volatiles were removed until ~7 mL remained. The solution was filtered, cooled to −78 °C, and filtered to yield 210 mg red-orange microcrystals (56%). ^1H NMR (C_6D_6): δ 1.25 (^{t}Bu, s, 81 H), 1.64 (t-*H*HC=, 1 H, ^2J = 10, ^3J = 12 Hz), 2.30 (-HC=, ddq, 1 H, ^3J = 12, ^3J = 16, ^3J = 7 Hz), 2.73 (CH_3, d, 3 H, ^3J = 7 Hz), 2.99 (c-H*H*C=, 1 H, ^2J = 10, ^3J = 16 Hz). $^{13}C\{^1H\}$ NMR: δ 23.47 (SiC), 26.64 (CH_3), 30.68 (CCH_3), 73.39, 77.83 (C=C). Anal. Calcd for $C_{39}H_{87}O_3Si_3Ta$: C, 53.88; H, 10.09. Found: C, 53.98; H, 10.02.

9. (silox)$_2$HTaOSi^{t}Bu$_2$CMe$_2$CH$_2$ (6). Crystalline (silox)$_3$Ta (1; 800 mg, 0.969 mmol) was stored at 25 °C for 6 weeks, resulting in a white powder that was recrystallized from 5 mL of THF at −78 °C to give 670 mg of waxy, colorless 6 (84%). ^1H NMR (C_6D_6): δ 1.27 (^{t}Bu, s, 54 H), 1.29 (^{t}Bu, s, 18 H), 1.37 (Me_2, s, 6 H), 1.89 (CH_2, s (br), 2 H), 21.97 (TaH, s, 1 H). $^{13}C\{^1H\}$ NMR (C_6D_6): δ 23.52 (Si(CMe_3)$_2$), 23.61 (silox SiC), 24.93 (CMe_2), 30.73 (silox Me), 33.61 (Si(C(CH_3)$_2$), 39.80 (C-(CH_3)$_2$), 97.04 (CH_2); $^{29}Si\{^1H\}$ NMR: δ 16.37 (silox), 20.43 (OSi^{t}Bu$_2$CMe$_2$CH$_2$). IR (Nujol): ν(Ta–H) = 1770 cm^{-1}. Anal. Calcd for $C_{36}H_{81}O_3Si_3Ta$: C, 52.27; H, 9.87. Found: C, 52.11; H, 9.72.

10. [(silox)$_3$Ta]$_2$[μ-η^2(1,2):η^2(4,5)-C$_6$H$_6$] (7). A vial containing 331 mg of (silox)$_3$Ta (1, 0.400 mmol) and 4 mL of C_6H_6 was allowed to stand for 2 weeks under an N_2 atmosphere in the drybox. The pale blue solution was filtered and the brown crystals washed with six 2-mL portions of benzene (23 mg, 7%). ^1H NMR (THF-d_8): δ 1.20 (^{t}Bu, s, 180 H), 4.80 (C_6H_6, s, 6 H (tentative)). $^{13}C\{^1H\}$ NMR: δ 24.17 (SiC), 31.53 (Me), 85.21 (μ-C_6H_6 (tentative)). Anal. Calcd for $C_{78}H_{168}O_6Si_6Ta_2$: C, 54.07; H, 9.77. Found: C, 53.84; H, 9.64.

11. (silox)$_3$Ta(η-C$_2$H$_2$) (8a). To a 25-mL flask containing 308 mg of (silox)$_3$Ta (1; 0.372 mmol) was distilled 12 mL of hexanes at −78 °C. The flask was opened to a calibrated gas bulb containing acetylene, which was separated from the acetone stabilizer by a dry ice trap (0.415 mmol, 1.12 equiv). No color change noticed until the solution was warmed to 25 °C at which time a pale yellow solution formed (30 min). The reaction was stirred for 12 h and concentrated to dryness. After the residue was dissolved in 3 mL of hexanes, the solution was heated to 80 °C under 1 atm of N_2 and left overnight. Filtration and isolation at −78 °C led to large colorless crystals (230 mg, 72%). ^1H NMR (C_6D_6): δ 1.24 (^{t}Bu, s, 81 H), 11.91 (CH, s, 2 H). ^{13}C NMR (C_6H_6): δ 23.45 (SiC, s), 30.65 (Me, q, J_{CH} = 125 Hz), 216.97 (CH, d, J_{CH} = 169 Hz). Anal. Calcd for $C_{38}H_{83}O_3Si_3Ta$: C, 53.49; H, 9.80. Found: C, 53.95; H, 9.96.

12. (silox)$_3$Ta(η-C$_2$Me$_2$) (8b). Into a glass bomb charged with (silox)$_3$Ta (1; 500 mg, 0.604 mmol) and 10 mL of benzene was distilled 0.8 mL of 2-butyne (~10 mmol) at 77 K. The bomb was closed and warmed to 25 °C, and the contents were stirred for 18 h. The solution was cloudy yellow. The volatiles were then removed and the residue washed from the bomb with 10 mL of hexanes. An insoluble white solid (possibly poly(2-butyne)) was removed from the hexane solution by filtration and the volume reduced to 1 mL. Five milliliters of Et_2O was added and the solution cooled to −78 °C to give a slurry of colorless crystals isolated by filtration (200 mg, 35%). ^1H NMR (C_6D_6): δ 1.27 (^{t}Bu, s, 81 H), 2.59 (Me, s, 6 H). $^{13}C\{^1H\}$ NMR (C_6D_6): δ 22.05 (Me_2), 23.37 (SiC), 30.68 (CCH_3), C≡C not observed. Anal. Calcd for $C_{40}H_{87}O_3Si_3Ta$: C, 54.51; H, 9.95. Found: C, 54.50; H, 9.89.

13. [(silox)$_3$Ti]$_2$(μ-C$_2$H$_4$) (9). To a flask containing (silox)$_3$Ti (2; 350 mg, 0.504 mmol) and 25 mL of hexanes was added 0.5 equiv of C_2H_4 (0.252 mmol) by calibrated gas bulb. The solution, originally clear orange, turned a cloudy yellow as a light yellow solid precipitated over a 5–10-min period at 23 °C. After the mixture was stirred at 23 °C for 1 h, the precipitate was filtered and washed with hexanes to give 300 mg (82%) of a fine yellow powder that was insoluble in hexanes, benzene, toluene, and Et_2O and virtually insoluble in THF. IR (Nujol, cm^{-1}): 1011 (w), 998 (w), 930 (w), 910 (m), 850 (s), 818 (s), 620 (s). Anal. Calcd for $C_{74}H_{166}O_6Si_6Ti_2$: C, 62.75; H, 11.81. Found: C, 62.98; H, 11.52.

14. (silox)$_3$Ta(η^2-NC$_5$H$_5$-*N*,*C*) (10a). To a 25-mL flask containing 306 mg of (silox)$_3$Ta (1; 0.370 mmol) was distilled 12 mL of hexanes at −78 °C. The flask was opened to a calibrated gas bulb containing pyridine (0.402 mmol, 1.09 equiv). An excess of pyridine may be used with the same results. The initial blue color was immediately discharged to give a yellow-orange solution; upon warming to 25 °C for 2 h, the solution darkened slightly. The solution was reduced to 3 mL, filtered, and cooled to −78 °C to yield large amber crystals (215 mg, 65%). IR (Nujol, cm^{-1}): 1596 (w), 1513 (w), 1227 (m), 1133 (m), 1017 (w, sh), 1007 (m), 960 (m), 933 (m), 857 (s), 823 (s), 713 (m), 654 (w), 624 (s). UV–vis [hexane; λ, nm (ε, M^{-1} cm^{-1})] 215 (20000), 250 (9000), 340 (2000). Anal. Calcd for $C_{41}H_{86}O_3Si_3NTa$: C, 54.33; H, 9.56; N, 1.55. Found: C, 54.50; H, 9.62; N, 1.62. M_r: found 876 (calcd 906).

15. (silox)$_3$Ta(η^2-6-NC$_5$H$_4$Me-*N*,*C*) (10b). To a 50-mL flask containing 318 mg of (silox)$_3$Ta (1; 0.384 mmol) was distilled 20 mL of hexanes at −78 °C. The flask was opened to a manifold containing an excess of 2-picoline (~3 Torr, ~5 mmol) until the initial blue color was discharged to give a yellow-orange solution. Upon warming to 25 °C for 2 h, the solution darkened slightly. After concentration to dryness and removal of excess picoline in vacuo, the solid was redissolved in 8 mL of hexanes. Reduction of the volume to 3 mL, cooling to −78 °C, and filtration led to the isolation of yellow-orange microcrystals (220 mg, 62%). Anal. Calcd for $C_{42}H_{88}O_3Si_3NTa$: C, 54.81; H, 9.64; N, 1.52. Found: C, 55.56; H, 9.67; N, 1.37.

NMR Tube Reactions. General Information. Five-millimeter NMR tubes were sealed to ₹ 14/20 ground glass joints. The samples were loaded into the tubes in the drybox and then freeze–pump–thaw degassed (77 K) three times and sealed off with a torch. In certain instances, it was more convenient to prepare the samples in small pots and transfer the complex to the NMR tube in the drybox.

1. (silox)$_3$TiL (L = 2-Picoline (2-2-NC$_5$H$_4$Me), 4-Picoline (2-4-NC$_5$H$_4$Me), 4-^{t}Bu-py (2-4-NC$_5$H$_4$^{t}Bu), 3,5-Lutidine (2-3,5-NC$_5$H$_3$Me$_2$)). To a solution of (silox)$_3$Ti (50 mg, 0.07 mmol) in 10 mL of hexanes was added the appropriate substituted pyridine (0.10–0.15 mmol) at −78 °C. On warming to 25 °C, the bright orange solution changed to deep purple-blue. The solvent and excess ligand were then removed, leaving a gummy dark blue solid. Then, 10 mL of fresh solvent was added to the solid and then removed, until the solid lost its gummy appearance (two to three cycles). The solid thus formed was not recrystallized prior to use in the spectroscopic studies.

2. (silox)$_3$Ta(η-C$_2$H$_3$Et) (5c). An NMR tube was charged with 20 mg of (silox)$_3$Ta (1, 0.024 mmol) and ~0.4 mL of C_6D_6. After the solution was degassed, 23 Torr of *cis*-2-butene (0.024 mmol) was condensed at 77 K from a gas bulb of known volume (19.4 mL). Monitoring of the reaction by ^1H NMR showed the conversion to 5c over a 19-h period (25 °C); <10% of 6 was present. ^1H NMR (C_6D_6): δ 1.25 (^{t}Bu,

s, 81 H), 1.44 (CH_3, t, 3 H, J = 7 Hz), 1.62 (t-*H*H=, dd, 1 H, J = 10, 11 Hz), 1.94 (CH*H*, m, 1 H), 2.22 (-HC=, m, 1 H), 2.73 (C*H*H, m, 1 H), 2.99 (c-H*H*C=, dd, 1 H, J = 10, 15 Hz). $^{13}C\{^1H\}$ NMR (C_6D_6): δ 22.78 (CH_3), 23.47 (SiC), 30.73 (C*C*H_3), 34.34 (CH_2), 71.98, 86.41 (C=C).

3. (silox)$_3$Ta(η-*cis*-HMeC=CHMe) (5d). An NMR tube was charged with 19 mg of (silox)$_3$Ta (**1**, 0.023 mmol) and ~0.5 mL of C_6D_6. After the solution was degassed, 180 Torr of *cis*-2-butene (0.23 mmol, 10.0 equiv) was condensed at 77 K from a gas bulb of known volume (24.0 mL). Upon thawing, no immediate color change was observed. After standing overnight, the solution became amber. Monitoring of the reaction by ^1H NMR revealed the conversion to **5d** over a 3-day period (25 °C); >10% of **6** was present. ^1H NMR (C_6D_6): δ 1.24 (^{t}Bu, s, 81 H), 1.26 (Me, s, 6 H), 2.66 (-HC=, s, 2 H). $^{13}C\{^1H\}$ NMR: δ 18.19 (CH*C*H_3), 23.41 (SiC), 30.74 (Me), 79.10 (C=C).

4. (silox)$_3$Ta(η-CF$_3$CCCF$_3$) (8c). An NMR tube was charged with 19 mg of (silox)$_3$Ta (**1**; 0.023 mmol) and ~0.4 mL of C_6D_6. After the solution was degassed, 19 Torr of CF_3CCCF_3 (0.02 mmol, 1.0 equiv) was condensed at 77 K from a gas bulb of known volume (19.6 mL). When the benzene thawed, immediate discharge of the blue color was observed to give a colorless solution. ^1H NMR (C_6D_6): δ 1.21 (^{t}Bu, s). $^{13}C\{^1H\}$ NMR: δ 23.34 (SiC), 30.53 (Me); the CF_3CCCF_3 carbons were not located. ^{19}F NMR: δ -54.74 (vs external $CFCl_3$ set to 0 ppm).

5. (silox)$_3$HTa($C_5H_2Me_2N$) (11a) and (silox)$_3$Ta(η^2-2,6-$NC_5H_3Me_2$-*N*,*C*) (11b). An NMR tube was charged with 22 mg of (silox)$_3$Ta (**1**; 0.027 mmol) and ~0.4 mL of C_6D_6. After the solution was degassed, 3 Torr of 2,6-lutidine (0.046 mmol, ~1.7 equiv) was condensed with a gas bulb of known volume (287.8 mL). After 20 min, a fading of the blue color was observed. The ^1H NMR showed unreacted **2**, free lutidine, and a single new compound (**11a**). ^1H NMR (C_6D_6): δ 1.25 (^{t}Bu, s, 81 H), 2.61 (Me_2, s, 6 H), 8.10 (CH, s, 2 H), 22.93 (TaH, s, 1 H). $^{13}C\{^1H\}$ NMR: δ 23.79 (SiC), 30.61 (C(*C*H_3)$_3$), 31.07 (Me_2), 130.04 (*C*Me), 156.99 (CH), 203.77 (C_{ipso}). After 8 h, the solution was yellow. The ^1H NMR (C_6D_6) showed unreacted **1**, 2,6-lutidine, **11a**, and **11b**.

6. (silox)$_3$Ta(η^2-$N_2C_4H_4$-*N*,*N'*) (12). To an NMR tube with a septum screw cap containing 18 mg of (silox)$_3$Ta (**1**; 0.022 mmol) was added 0.5 mL of C_6D_6. One equivalent of pyridazine (1.6 μL, 0.022 mmol) was added via syringe, and the blue solution immediately turned wine-red, indicative of **12**. After ~5 h, **12** totally degraded as indicated by the formation of a yellow solution and concomitant white precipitate.

7. (silox)$_3$Ta(η^2-1,6-$N_2C_4H_4$-*N*,*C*) (13). To an NMR tube with a septum screw cap containing 18 mg of (silox)$_3$Ta (**1**; 0.022 mmol) was added 0.5 mL of C_6D_6. One equivalent of pyrimidine (1.7 μL, 0.022 mmol) was added via syringe, and the blue solution immediately turned rust-colored, with a small amount of a concomitant reddish precipitate. Centrifugation yielded a clear, orange solution of **13** for spectroscopic studies.

Physical Studies. 1. Pyridine Exchange Kinetics of 10a. Four stock solutions were prepared in 2-mL volumetric flasks with 60 mg (0.066 mmol) of (silox)$_3$Ta(η^2-NC_5H_5-*N*,*C*) (**10a**), 3 drops of hexamethyldisiloxane (internal standard), pyridine-d_5 in varying amounts, and C_6D_6. The pyridine-d_5 was added by microliter syringe in 10 (53 μL), 40 (212 μL), 70 (371 μL), and 100 (530 μL) equiv amounts. For each run, three NMR tubes were charged with 0.6 mL of the prepared stock solution, degassed three times, and sealed off with a torch. The kinetics were run at 53.7 ● 0.1 °C in a polypropylene bath and the exchange monitored by ^1H NMR. The disappearance of the resonances at δ 5.73, 5.22, and 3.89 were followed because they were not obstructed by the benzene solvent peak or the appearance of free pyridine resonances. The rates of decay for each resonance in the three tubes (nine total) were averaged to obtain the final value at each concentration. The rate constants were obtained via linear, nonweighted fits to the logarithmic form of the rate expression.

2. Curie Plots (δ vs $1/T$) for (silox)$_3$Ti(py) (2-py). Spectra were recorded on a Varian XL-400 instrument over a temperature range of +60 to -90 °C, with a line broadening of 5–10 Hz. The silox ^{t}Bu resonances were supressed with a homonuclear decoupling sequence to allow better resolution of the pyridine resonances. Chemical shifts were monitored until the breadth of the peak precluded accurate measurement. Plots of the chemical shift vs $1/T$ were highly linear for all three ring positions (2,6, r^2 = 0.997; 3,5, r^2 = 0.999; 4, r^2 = 0.999) and approached 0 in the limit of $T \rightarrow \infty$.[67]

3. Equilibrium Study of (silox)$_3$Ti(2-NC_5H_4Me) (2-2-NC_5H_4Me). A series of NMR tubes with varying concentrations of (silox)$_3$Ti (**2**) was made as follows: To NMR tubes sealed to Ŧ 14/20 joints were added 0, 5, 20, 35, 50, and 65 mg of **2**. To each tube was added 0.7 mL of a 0.045 M solution of 2 picoline in toluene-d_8. The tubes were degassed and sealed with a torch. Spectra were acquired at 0.7, 20.0, 40.0, and 60.0 °C. Below 20 °C, the higher concentration tubes showed precipitation of 2-2-NC_5H_4Me, so those tubes were not included in the data set for 0.7 °C. Plots of $1/[Ti]$ vs. $1/(\delta_{obs} - \delta_f)$ showed some deviation from linearity (r^2 = 0.92–0.98; δ_f = chemical shift of the Me resonance of the free ligand).[70,71] A nonlinear fit of K and δ_b (δ_b = chemical shift of the Me resonance of the bound ligand) from δ_{obs} and [Ti] did not give significantly different results. The values for the equilibrium constant at each temperature derived from the nonlinear fit were used to calculate ΔH and ΔS for the association.

4. Magnetic Studies of [(silox)$_3$Ta]$_2$(μ-η^2(1,2):η^2(4,5)-C_6H_6) (7). Magnetic measurements were performed by the Faraday method[83–86] with $HgCo(SCN)_4$ as a calibrant (16.44×10^{-6} emu/g at 298 K). A detailed description of the instrument and the operational software is available.[86] A sealed bucket system, enabling sample loading in a drybox, was utilized for **7**. Samples were transferred to the balance by using an O-ring-sealed container. All measurements were corrected for the bucket force, shown to be temperature independent, and for sample diamagnetism by using standard Pascal constants.[34] A room-temperature measurement indicated the complex was diamagnetic with χ_m (296 K) = -6.1×10^{-4} emu/mol, using the diamagnetic correction of -1371.4×10^{-6} emu/mol.

Extended Hückel (EHMO) Calculations. Parameters were taken from previous works.[49,87]

Acknowledgment. Primary support from the Air Force Office of Scientific Research (Grant AFOSR-87-0103) and the National Science Foundation (Grant CHE-8714146) are gratefully acknowledged as are contributions from the Union Carbide Innovation Recognition Program and Cornell University. We thank John F. Mitchell and Dr. Lászlő Párkányi for the X-ray studies of **7** and **10a**,[24] Profs. David B. Collum, Klaus H. Theopold, and Robert Scott for helpful discussions, Dr. Darrin S. Richeson for magnetic measurements, A. W. Edith Chan for EHMO heterocycle calculations and veteran UV–vis sharpshooter Prof. Harry B. Gray for aid in interpreting the spectrum of (silox)$_3$Ta (**1**). Support for the Cornell NMR Facility from the NIH and NSF Instrumentation Programs is acknowledged.

(83) Bates, L. F. *Modern Magnetism*, 3rd ed.; Cambridge University Press: London, 1951.
(84) Kulick, J. D.; Scott, J. C. *J. Vac. Sci. Technol.* **1978**, *15*, 800–804.
(85) Morris, B. L.; Wold, A. *Rev. Sci. Instrum.* **1968**, *39*, 1937–1941.
(86) Richeson, D. S. Ph.D. Thesis, Cornell University, 1988.
(87) Lauher, J. W.; Hoffmann, R. *J. Am. Chem. Soc.* **1976**, *98*, 1729–1742.